NATIONAL ADVISORY COMMITTEE FOR AERONAUTICS

TECHNICAL NOTE 4176

EFFECT OF FLOW INCIDENCE AND REYNOLDS NUMBER ON LOW-SPEED AERODYNAMIC CHARACTERISTICS OF SEVERAL NONCIRCULAR CYLINDERS WITH APPLICATIONS TO DIRECTIONAL STABILITY AND SPINNING

By Edward C. Polhamus

Langley Aeronautical Laboratory
Langley Field, Va.

Washington
January 1958

NATIONAL ADVISORY COMMITTEE FOR AERONAUTICS

TECHNICAL NOTE 4176

EFFECT OF FLOW INCIDENCE AND REYNOLDS NUMBER ON LOW-SPEED AERODYNAMIC CHARACTERISTICS OF SEVERAL NONCIRCULAR CYLINDERS WITH APPLICATIONS TO DIRECTIONAL STABILITY AND SPINNING

By Edward C. Polhamus

SUMMARY

The aerodynamic characteristics of several noncircular two-dimensional cylinders with axes normal to the stream at various flow incidences (analogous to angles of attack of a two-dimensional airfoil and obtained by rotating the cylinders about their axes) for a range of Reynolds numbers have been determined from low-speed wind-tunnel tests. The results indicate that these parameters have rather large effects on the drag and side force developed on these cylinders. The side force is especially critical and very often undergoes a change in sign with a change in Reynolds number. Since the flow incidences correspond to combined angles of attack and sideslip in the crossflow plane of three-dimensional bodies, these two-dimensional results appear to have strong implications with regard to directional stability of fuselages at high angles of attack. These implications, along with those associated with the spin-recovery characteristics of aircraft, are briefly discussed.

INTRODUCTION

Because of the current trend toward low-aspect-ratio wings and large-volume fuselages with long nose lengths, the relative importance of the fuselage contribution to the aerodynamic characteristics of aircraft configurations is increasing rapidly. In addition, considerations such as inlet locations, engine installations, and wing-fuselage interference have led to a variety of fuselage cross sections. As indicated in reference 1, for example, cross section can have considerable effect on both the longitudinal and lateral aerodynamic characteristics, especially at high angles of attack. Large effects of cross section have also been observed in spin investigations such as that reported in reference 2 where the cross section of the fuselage afterbody was varied. In view

of the trend toward increased fuselage length ahead of both the center of gravity and the wing, it might be expected that the spin characteristics of current aircraft would be affected to an even greater extent by changes in forebody cross section. Although the effects of fuselage cross section on the flow field in the vicinity of the empennage have large effects on stability, large effects have also been traced to direct fuselage forces. Thus, a better understanding of the effect of cross section on the fuselage forces, especially at combined angles of attack and sideslip, is believed to be of value to the aircraft designer. Since, even for circular cross sections, a large part of the forces encountered are associated with crossflow separation, it would appear that empirical methods, such as those developed in references 3 and 4, must be resorted to at the present time. In these methods the flow past the body is resolved into two components, one parallel to the body axis and one normal to it. It is then assumed that the crossflow is independent of the axial flow and therefore related to the flow about a cylinder at right angles to the flow. However, for the extremely high angles of attack often encountered in spins, the problems involving the degree of interdependence between the crossflow and axial flow (see ref. 5) are largely eliminated. For both these methods, it is necessary to have a knowledge of the forces on a two-dimensional cylinder normal to the flow and having the same cross section as the fuselage in question. For a circular fuselage at any attitude or noncircular fuselages in a pure pitch or sideslip attitude, only the crossflow drag of the corresponding cylinder need be known, and a considerable amount of this information is available (refs. 6 and 7). However, for noncircular fuselages at combined angles of attack and sideslip, the resultant force on the equivalent cylinder at a flow incidence corresponding to the combined angle of attack and sideslip must be known. For the most part, available two-dimensional-cylinder data for shapes other than airfoil and elliptical (ref. 8) are limited to zero flow incidence. One exception is the results for the triangular cylinder of reference 7; however, these data are limited to rather low Reynolds numbers.

The purpose of the present investigation, therefore, is to determine the forces on several noncircular two-dimensional cylinders with axes normal to the stream at various flow incidences (analogous to angles of attack of a two-dimensional airfoil and obtained by rotating the cylinders about their axes) for a range of Reynolds numbers and to make a limited correlation with three-dimensional bodies at combined angles of attack and sideslip.

SYMBOLS

The convention used with regard to flow inclination, cylinder reference dimensions, and the direction and positive sense of the aerodynamic coefficients are presented in figure 1. The aerodynamic coefficients and

Reynolds numbers have been corrected for the effects of the wind-tunnel walls by the method of reference 9. The definitions of the symbols used throughout the paper are as follows:

A	maximum fuselage cross-sectional area
b	maximum projected width of cylinder normal to flow for given flow incidence
b_o	maximum width of cylinder normal to flow at zero flow incidence
c_d	section drag coefficient, $\frac{\text{Force in stream direction per unit length}}{b\frac{\rho}{2}V_n^2}$
C_n	yawing-moment coefficient of fuselage
c_o	maximum depth of cylinder parallel to flow at zero flow incidence
c_x	section longitudinal-force coefficient, $\frac{\text{Longitudinal force per unit length}}{b_o\frac{\rho}{2}V_n^2}$
C_Y	side-force coefficient of fuselage, $\frac{\text{Side force}}{\frac{\rho}{2}V^2A}$
c_y	section side-force coefficient, $\frac{\text{Side force per unit length}}{b_o\frac{\rho}{2}V_n^2}$
c_y'	section side-force coefficient based on c_o
D	maximum diameter of fuselage
L	total length of fuselage
l	length of fuselage rearward of center of gravity
M	Mach number
R	Reynolds number
r	corner radius

S	effective side area of fuselage
V	free-stream velocity for three-dimensional bodies
V_n	free-stream velocity for cylinders normal to flow (see fig. 1) or velocity component normal to axis of three-dimensional body
x,y,z	Cartesian coordinates of fuselage (see table I)
α	angle of attack of fuselage
β	angle of sideslip of fuselage
ρ	free-stream air density
ϕ	angle of flow incidence in plane normal to axis of two-dimensional cylinder or three-dimensional body
Ω	rate of spin

MODELS AND EQUIPMENT

Details of the cross section of each cylinder tested are presented in figure 2(a), and a photograph (taken from the downstream side) of the cylinder having a modified triangular cross section mounted in the wind tunnel is shown in figure 2(b). The models were constructed of mahogany and were lacquered to produce smooth surfaces. The square cylinder having the small corner radii was made considerably larger than the other cylinders in order to make possible the attainment of supercritical Reynolds numbers, which would be expected to be considerably higher for this shape than for the cross sections having the larger radii (ref. 6).

The cylinders were tested in the Langley 300-MPH 7- by 10-foot tunnel, and they spanned the tunnel from floor to ceiling (fig. 2(b)). In order to minimize any effects which might be caused by air leakage through the small clearance gaps where the cylinders passed through the floor and ceiling, each of the cylinders was equipped with an end plate (fig. 2(b)). The forces and moments developed on the cylinders were measured by means of a mechanical balance system.

In order to determine the degree to which the side-force characteristics of the two-dimensional cylinders might be indicative of the directional stability characteristics of three-dimensional bodies at high angles of attack, three fuselages were also tested in the 300-MPH

7- by 10-foot tunnel. Details of the fuselages, all of which had the same longitudinal distribution of cross-sectional area, are presented in table I. The fuselages had constant sections from $\frac{x}{L} = 0.3200$ to $\frac{x}{L} = 0.7534$, and for the rectangular fuselages the sections were identical to those of the two-dimensional cylinders. Forward and rearward of this constant section, there was a gradual transition to a circular cross section.

RESULTS

The basic data are presented in figures 3 to 8 as a function of Reynolds number. The circular cylinder was included in the investigation to provide an end point for the corner-radius series and to afford a comparison with previous investigations to determine whether any serious interference effects existed near the walls because of the gaps and end plates. The results for the circular cylinder of the present investigation are compared with the results of references 10 and 11 and the agreement shown (see fig. 3) indicates that no serious interference effects existed, and this fact is also assumed to be true for the noncircular cylinders of the present investigation. Because of the small size of the cylinder of reference 11, supercritical Mach numbers ($M > 0.4$) were encountered at Reynolds numbers beyond that indicated by the tick.

The basic data for the noncircular cylinders are presented in figures 4 to 8, where both the section longitudinal-force coefficient c_x and the section side-force coefficient c_y are presented as functions of Reynolds number for various angles of flow incidence ϕ. The body axes rather than the wind axes were used for presentation of the data in order to simplify the estimation of the stability characteristics of fuselages, since the currently preferred practice is to relate fuselage characteristics to the body axes. It is important to keep in mind that for all the basic data (figs. 4 to 8) the aerodynamic coefficients are based on b_o, the maximum cylinder width normal to the stream at $\phi = 0^\circ$ (fig. 1). Although the side force at small and moderate flow incidences is usually more dependent upon the depth c_o, the width was used to provide consistency between c_x and c_y. However, in some of the summary figures, the side-force coefficients are based on c_o in order to illustrate certain points and these coefficients will be indicated by the use of a prime.

Data for the square cylinders were obtained only for flow incidences up to $\phi = 45^\circ$ inasmuch as the data for other angles can be obtained by

properly converting the angles and forces. However, for the rectangular and triangular cylinders, data had to be obtained up to $\phi = 90^\circ$. In presenting the data for the rectangular cylinder, however, it was believed that application to fuselages at high angles of attack might be facilitated by presenting the data for flow-incidence ranges from 0° to 45° for a rectangular cylinder with its major axis parallel to the stream (corresponding to a deep fuselage) at $\phi = 0^\circ$ and for a rectangular cylinder with its major axis normal to the stream (corresponding to a shallow fuselage) at $\phi = 0^\circ$. Of course, data for the complete range of flow incidences can be obtained by converting incidence angles, exchanging force coefficients, and correcting for the coefficient reference lengths.

The Reynolds number used throughout the present investigation is based on the velocity V_n and on the maximum depth of the cylinder parallel to the velocity at $\phi = 0^\circ$.

It should be pointed out that the Reynolds number variation was obtained during the increasing-velocity portion of the test. As the tunnel velocity was reduced, however, a hysteresis effect was sometimes observed which appeared to reduce the critical Reynolds number by as much as 200,000 in some cases. Since it was rather difficult to hold the tunnel velocity in the region of the critical Reynolds number, the velocity pulsations combined with the hysteresis effect may have had some effect on the plateau observed in the data in the transition region. (See figs. 4(a) and 4(b).)

DISCUSSION

In this section, a limited discussion of the application of the results of this investigation is presented. This discussion consists of some brief remarks with regard to the effects of Reynolds number and cross section on the drag and side-force coefficients of two-dimensional cylinders and the implications of these results with regard to the stability of aircraft at large angles of attack such as those encountered in spins.

Drag of Two-Dimensional Cylinders

The section drag coefficient of square cylinders of various corner-radius ratios (r/b_o) at $\phi = 0^\circ$ are plotted against Reynolds number in figure 9(a). The results for the cylinders having $\frac{r}{b_o} = 0.080$ and 0.245 are from the present investigation, whereas the results for the other cylinders were obtained from reference 6. The results presented in the

upper plot of figure 9(a) indicate a rather large effect of corner radius on both the section drag coefficient and the critical Reynolds number; both increase as the radius is decreased. This increase is, of course, associated with the more pronounced separation at the corners caused by the increasing severity of the adverse pressure gradients as the radius is reduced. The rather large effect of radius on the critical Reynolds number makes it somewhat difficult to predict, by interpolation, the drag variation for radii other than those presented. In an attempt to alleviate this situation, the critical Reynolds numbers have been forced to coincide by means of an empirical factor applied to the Reynolds number, and the data have been replotted in the lower part of figure 9(a). It appears that, for the usual engineering accuracy required, only a vertical interpolation need be made to obtain the drag variation for any radius between $\frac{r}{b_o} = 0.080$ and 0.333.

Figure 9(b) presents the results for the diamond cylinders - that is, the same square cylinders rotated 45° to the stream. Although the section drag coefficient is based on the maximum width normal to the stream b, the corner radii are nondimensionalized by b_o for convenience in comparing the results with those from figure 9(a). For this condition, it will be noted that, although the corner radius has a large effect on the critical Reynolds number, it has only a slight effect on the magnitude of the section drag coefficient at subcritical Reynolds numbers, at least for values of r/b_o less than 0.333. The subcritical drag characteristics of the diamond cylinders are therefore considerably different from those of the square cylinders. Also, the drag characteristics of the circular cylinder are more similar to those of the diamond cylinders (fig. 9(b)) than those of the square cylinders (fig. 9(a)). For example, both the circular and diamond cross sections exhibit a gradual transition from subcritical to supercritical flow conditions, whereas the square cylinders exhibit a rapid transition for the range of radii investigated. Some of these observations may be explained, to some extent at least, by the theoretical pressure distributions presented in figure 10. These distributions were calculated by the method of reference 12. The pressure distributions indicate, as might be expected, that the general character of the flow about the diamond cross section with round corners is considerably more similar to the flow about the circular cross section than about the square cross section with round corners. In view of this similarity, it is not surprising that the general drag characteristics of the circular cylinder are similar to those of the diamond series. The extreme adverse pressure gradients encountered on the diamond cross section, despite large corner radii, would lead one to believe that the breakaway point is very near the position of maximum width and probably accounts for the fact that the subcritical drag is relatively independent of corner radius and is considerably higher than that for the circular cylinder (fig. 9(b)). The transition in subcritical drag characteristics

between the square cylinders, which are extremely sensitive to corner radius, and the diamond cylinders, which are relatively insensitive to corner radius, is shown in figure 11. In this figure the section drag coefficient, which is based on the respective maximum projected widths normal to the flow b, is plotted as a function of the incidence of flow ϕ for various corner radii; the square cylinders correspond to $\phi = 0^\circ$ and the diamond cylinders correspond to $\phi = 45^\circ$. In addition to the results of the present investigation, the variation of c_d with ϕ for sharp corners $\left(\frac{r}{b_o} = 0\right)$, as obtained from reference 13, is presented. The results from reference 6, which were obtained only for $\phi = 0^\circ$ and 45°, are also presented. The data indicate a rather rapid reduction in drag associated with an increase in incidence ϕ over a moderate range with the minimum drag occurring at different values of ϕ depending upon the corner radius. The effect of corner radius diminishes rapidly as the drag rises beyond the incidence for minimum drag, and for incidences above about 30° there is essentially no effect of corner radius.

For the drag characteristics of cylinders having other shapes, the reader is referred to figures 6, 7, and 8 and references 6, 7, and 8.

Side Force Developed on Two-Dimensional Cylinders

A knowledge of the side forces developed on various two-dimensional cylinders for a range of flow incidences and Reynolds numbers might be valuable in predicting, at least qualitatively (by crossflow methods similar to those of refs. 3 and 4), the directional stability characteristics of aircraft fuselages at high angles of attack. This information should be particularly useful in the case of spinning where extremely high angles of attack are often encountered, since for these conditions the effect of the axial flow on the crossflow is minimized. It should be kept in mind that the flow-incidence angle ϕ corresponds to the incidence of the crossflow component of the free-stream velocity about a three-dimensional body at various combinations of angle of attack α and angle of sideslip β. For example, at a given angle of sideslip, a small value of ϕ corresponds to a large angle of attack whereas a large value of ϕ corresponds to a small angle of attack. The actual relationships will be discussed in the section entitled "Directional Stability and Spinning Characteristics of Three-Dimensional Bodies."

In figures 4 to 8, the basic section data obtained for the various noncircular two-dimensional cylinders shown in figure 2(a) are presented as a function of Reynolds number for various values of the flow incidence ϕ. Note that Reynolds number, cross section, and flow incidence all have a rather large effect on the side force developed by two-dimensional cylinders. Some of the more striking effects are illustrated

in figure 12, where comparisons of various cross sections are made for a flow incidence of 10°. In the upper plot of figure 12(a) the variation of section side-force coefficient with Reynolds number is presented for the two square cylinders - one having a corner-radius ratio (r/b_o) of 0.080 and the other having a corner-radius ratio of 0.245. The results indicate that positive values of side-force coefficient (corresponding to a negative lift-curve slope for a two-dimensional airfoil) are developed at the lower Reynolds numbers for both of the square cylinders. Above a Reynolds number of about 650,000, the square cylinder having the corner-radius ratio r/b_o of 0.245 develops a large negative side-force coefficient (corresponding to a positive lift-curve slope) which is in fair agreement with the theory for a flat plate $(-2\pi \sin \phi)$.

The large effect of Reynolds number can be qualitatively explained by the following sketches which are based on tuft surveys:

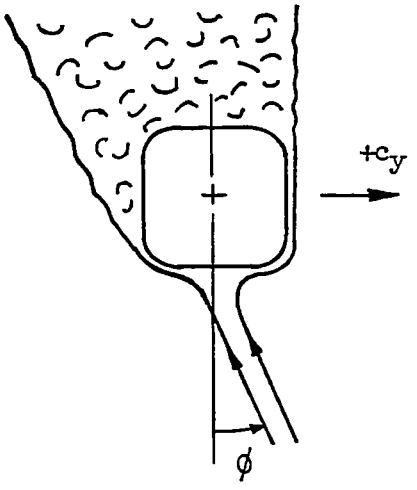

Subcritical Reynolds number

Sketch (a)

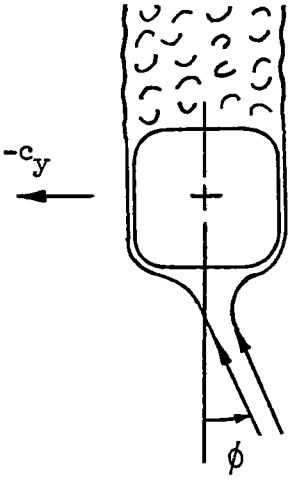

Supercritical Reynolds number

Sketch (b)

The surveys indicate that, at subcritical Reynolds numbers (sketch (a)), the flow separates at the left leading corner because of the strong adverse pressure gradient and that the stream is deflected in a direction which produces a force into the cross-wind component $(+c_y)$. However, at supercritical Reynolds numbers (sketch (b)), the flow remains attached and is deflected an amount approximately equal to the angle of flow incidence ϕ, as indicated by both the tuft surveys and the agreement with the flat-plate theory $(-2\pi \sin \phi)$. The adverse gradients are considerably more severe for the square cylinders having the sharper corners

$\left(\frac{r}{b_o} = 0.080\right)$ than for those having values of $\frac{r}{b_o}$ of 0.245; therefore, the separated flow persists to a much higher Reynolds number (fig. 12(a)). Although supercritical Reynolds numbers are not attained for the cylinder with $\frac{r}{b_o} = 0.080$, the results indicate that transition begins at a Reynolds number of about 1,500,000, and, at the highest Reynolds number attained, the section side-force coefficient has decreased to almost zero. It is interesting to note that the critical Reynolds number, if based on corner radius, would be approximately the same for the two cylinders.

The results presented in the lower part of figure 12(a) indicate that the section side-force characteristics for the triangular cylinder are considerably different from those of the square cylinders. At low Reynolds numbers a small negative side-force coefficient occurs, whereas at the higher Reynolds numbers a fairly large positive side-force coefficient occurs. This general trend is opposite to that observed for the square cylinders and might be explained by the following sketches which are based on tuft studies:

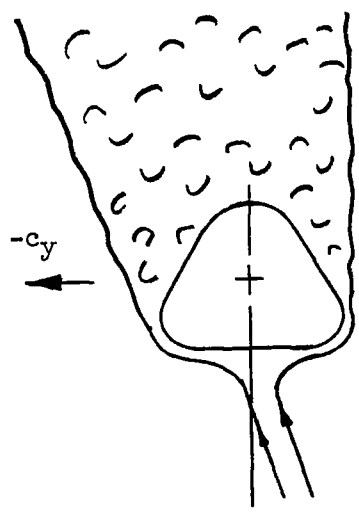

Subcritical Reynolds number

Sketch (c)

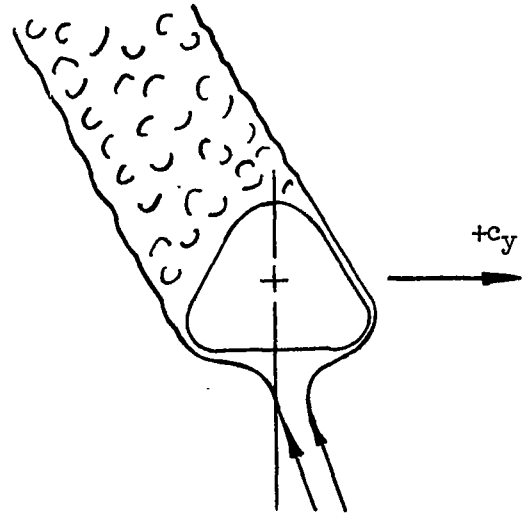

Supercritical Reynolds number

Sketch (d)

At subcritical Reynolds numbers (sketch (c)), the flow separates at both leading corners, and only a small negative side-force coefficient is developed. However, at supercritical Reynolds numbers, the flow attaches on the right-hand corner (sketch (d)), which has the least adverse pressure gradient, and is deflected in a direction that produces a positive

side force. Note that the flow is deflected in the same direction by the triangular cylinder at supercritical Reynolds numbers (sketch (d)) as by the square cylinder at subcritical Reynolds numbers (sketch (a)) and this fact apparently accounts for the opposite trends with Reynolds number between the two cross sections.

Figure 12(b) presents the variation of section side-force coefficient with Reynolds number for the cylinders having diamond and rectangular cross sections at a flow incidence of 10°. The results obtained with the diamond cross sections (see upper plot of fig. 12(b)) show relatively little effect of Reynolds number, and, as might be expected, the side-force characteristics are somewhat similar to those of the triangular cylinder (see lower plot of fig. 12(a)). The lower plot of figure 12(b) presents a comparison of the results obtained for the two rectangular cylinders and for the square cylinder; the trends with Reynolds number are essentially the same for all three cylinders. The flow studies previously presented for the square cylinder apparently also apply for the rectangular cylinders; therefore, no further discussion will be given except to point out again that the changes in critical Reynolds numbers are associated with the fact that the Reynolds numbers in the present investigation are based on c_o rather than corner radius. In order to illustrate this fact, the results for the square and rectangular cylinders are presented as a function of Reynolds number based on corner radius in figure 12(c).

In figure 12, side-force results were presented for only one angle of flow incidence. Figure 13 summarizes the variation of section side-force coefficient with flow incidence for all the cylinders of the present investigation and for those of references 7, 8, and 14. Results, where available, are shown for Reynolds numbers of 1,000,000 and 200,000. Also shown is the theoretical value for a flat plate $\left(\frac{-2\pi \sin \phi}{\sqrt{1 - M^2}}\right)$. The top plots of figure 13 show the changes in the variation of side-force coefficient with flow incidence as the cross section gradually changes from a rectangle with major axis normal (when $\phi = 0°$) to the flow to an NACA 0015 airfoil section alined (when $\phi = 0°$) with the flow. At the lower Reynolds number the curve for the initial rectangular cross section differs greatly from the theoretical curve for the flat plate, but this difference diminishes as the airfoil section is approached. The results also indicate that at the higher Reynolds number the variation of c_y' with ϕ approaches that for the flat plate regardless of cross-sectional shape. Although interesting observations can also be made with regard to the results presented in the bottom of figure 13, they are not discussed here since they will be considered in connection with application to directional stability.

Directional Stability and Spinning Characteristics of Three-Dimensional Bodies

In order to illustrate the degree to which the side-force characteristics of the two-dimensional cylinders might be indicative of the directional stability characteristics of three-dimensional bodies at high angles of attack, tests have been made on one circular-cross-section fuselage and on two rectangular-cross-section fuselages. The fuselages (see table I) were tested at an angle of sideslip of 5° through an angle-of-attack range from 0° to 24°, and the side-force coefficient (based on maximum cross-sectional area) developed is presented in the upper plot of figure 14. The side-force coefficient, rather than the yawing-moment coefficient, was selected because the yawing moment is dependent upon the particular moment reference point selected and because existing methods of applying two-dimensional data to three-dimensional bodies appear to be more successful with regard to the overall force than with regard to the distribution of the force (fig. 9 of ref. 15). The results indicate that the side force developed by the fuselage having a circular cross section was relatively independent of angle of attack. However, the side force developed by the fuselages having rectangular cross sections was greatly dependent upon angle of attack, especially for the rectangular fuselage with the major axis vertical and this result is in general agreement with the trends indicated in reference 1. It should be mentioned that for current aircraft, with their long fuselage noses and short tail lengths, the side-force characteristics indicated for the rectangular fuselages would tend to increase the fuselage directional instability at high angles of attack and supercritical crossflow Reynolds numbers.

The side-force variation for the three fuselages, as estimated with the aid of the two-dimensional-cylinder data, is presented in the lower part of figure 14. It should be pointed out that, for the subcritical crossflow Reynolds numbers which existed in the three-dimensional tests, the side forces developed on the two-dimensional cylinders would result in a trend with angle of attack opposite to that encountered on the three-dimensional bodies and that it was necessary to use supercritical values to obtain a reasonable correlation. This fact, however, is not surprising in view of the rather large degree of interdependence between the crossflow and the axial flow observed in references 4 and 5 for angles of attack up to 30° or 40°. Although considerable variation exists between the measured and estimated side forces for each of the rectangular fuselages, the general trend, with regard to the effect of fuselage cross section, appears to be sufficiently well defined to allow the use of two-dimensional cylinder data in the selection of fuselage cross sections. Also, a more rigorous method of applying the two-dimensional data might be expected to result in better agreement. In view of the shortcomings

of the methods currently available, the use of the simplified method was believed to be justified. In this method it was assumed that the small potential force on the boattailed afterbody, as predicted by theory, was not attained because of afterbody separation. The potential-flow contribution to the side force was therefore restricted to the expanding section of the nose, and the potential side-force coefficient is given by the following expression (ref. 3):

$$(C_Y)_{potential} = -\frac{2\beta}{57.3} \tag{1}$$

The side-force coefficient is based on the maximum cross-sectional area of the fuselage. In using the two-dimensional cylinder data to estimate the nonpotential side force contributed by the crossflow, it is necessary to relate the angles of attack and sideslip and the free-stream dynamic pressure of the three-dimensional body to the crossflow incidence and dynamic pressure as indicated in sketch (e). From this sketch, it can be seen that

$$\tan \phi = \frac{\tan \beta}{\sin \alpha}$$

Also, inasmuch as $q = \frac{1}{2}\rho V^2$ and $q_n = \frac{1}{2}\rho V_n^2$, then

$$q_n = q\left(\cos^2\beta \sin^2\alpha + \sin^2\beta\right)$$

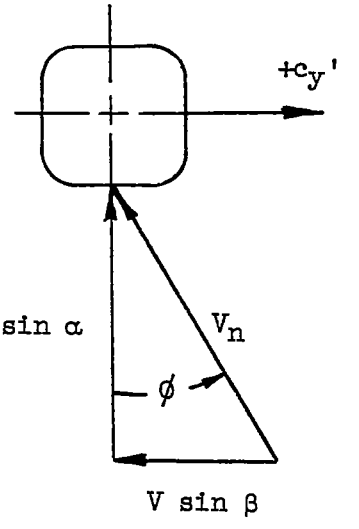

Sketch (e)

From these relationships, the nonpotential side-force coefficient can be written as follows:

$$(C_Y)_{nonpotential} = \frac{c_y' S\left(\cos^2\beta \sin^2\alpha + \sin^2\beta\right)}{A} \tag{2}$$

where S is an effective side area of the fuselage and c_y' is the two-dimensional side-force coefficient corresponding to ϕ and can be obtained

from figure 13 or from the basic data plots presented in figures 4 to 8. $\left(\text{In using figs. 4 to 8, it must be kept in mind that } c_{y'} = c_y \frac{b_o}{c_o}.\right)$ Adding equations (1) and (2) gives for the total side-force coefficient

$$C_Y = -\frac{2\beta}{57.3} + \frac{c_{y'}S\left(\cos^2\beta \sin^2\alpha + \sin^2\beta\right)}{A} \tag{3}$$

For the special case of circular cross sections,

$$c_{y'} = c_d \sin \phi$$

and

$$C_Y = -\frac{2\beta}{57.3} + \frac{c_d S}{\pi D^2/4} \sin \beta \sqrt{\cos^2\beta \sin^2\alpha + \sin^2\beta} \tag{4}$$

The best method of selecting the effective side area S for the various fuselages is not obvious. The results presented in reference 15 for fuselages having circular cross sections indicate that, because of the favorable pressure gradients, little crossflow separation occurs on the expanding section of the nose. Therefore, it would appear that for circular fuselages the side area rearward of the nose tangency point might be a reasonable approximation. However, for the rectangular fuselages the favorable gradients on the nose may increase the chances of encountering (even at low crossflow Reynolds numbers) the large side forces encountered on the two-dimensional cylinders at supercritical Reynolds numbers. This, in addition to the fact that the adverse gradients over the tapered afterbody probably deter the development of the large side forces, would suggest the use of the side area ahead of the tapered afterbody for the rectangular fuselages.

If the direct fuselage forces for current aircraft, with their long fuselage noses and short tail lengths, are contributed mainly from the portion of the fuselage ahead of the wing, then it would be desirable from a static-directional-stability standpoint to employ a cross section which develops a positive slope of C_Y against ϕ. When only the high Reynolds number results of figure 13 are considered, the square cross section with $\frac{r}{b_o} = 0.080$ and the triangular cross section with rounded corners appear to be the most desirable cross sections of those tested with regard to static directional stability at high angles of attack.

As previously pointed out, the axial flow is important for angles of attack up to 30° or 40°; however, for higher angles of attack, such as encountered often in spins, the axial flow has relatively little effect on the crossflow characteristics. Thus, for certain cross sections, considerable difference between model and flight spin characteristics could possibly be encountered because of the differences in crossflow Reynolds number. From figure 13, it appears that the rectangular and square cross sections with corner radii would be particularly susceptible to scale effects. Although comparisons between model and flight tests are not available for these cross sections, low-scale tests of fuselages having rectangular and elliptical cross section (ref. 2) tend to substantiate the applicability of the two-dimensional data and, therefore, reinforce somewhat the possibility of important scale effects. Figure 15 presents the results of the spin tests of reference 2 along with the results of the two-dimensional cylinders. In the upper part of figure 15 the yawing-moment coefficient due to spinning is presented as a function of the rate of spin for fuselages having rectangular and elliptical afterbodies. The damping moment is considerably less for the rectangular than for the elliptical afterbody, and at the lower spin rates a propelling moment is probably generated for the rectangular afterbody. This result is in qualitative agreement with the results for the two-dimensional cylinders of the present investigation, as can be seen from the lower part of figure 15. The side-force coefficient developed on rectangular and elliptical cylinders at flow incidences corresponding to those encountered at the base of the fuselage during the spin is presented and it will be noted that the characteristics are similar to those obtained in the spin. The results presented in figure 13, however, indicate that the particular effects of cross section indicated in figure 15 would be essentially eliminated at a crossflow Reynolds number of 1,000,000. Considerable care must therefore be exercised in predicting spin-recovery characteristics from tests of the model at low Reynolds number. With regard to the cross-sectional shapes that might be desirable from the standpoint of spin recovery, those having negative slopes of side force against angle of incidence would be expected to provide aerodynamic damping and would, therefore, be desirable. This side-force requirement is, of course, opposite to that discussed previously for static directional stability contributed by the forebody, and, based on results at a Reynolds number of 1,000,000, it appears that sharp leading corners as well as diamond and triangular cross sections should be avoided. However, verification is needed at Reynolds numbers closer to those encountered in flight.

CONCLUDING REMARKS

The results obtained from tests of various two-dimensional cylinders indicated that flow incidence, Reynolds number, and cross-sectional shape

have rather large effects on their aerodynamic characteristics. The side force developed is especially critical and very often undergoes a change in sign with a change in Reynolds number. These side forces, which can be very large, appear to have rather strong implications with regard to directional stability characteristics of three-dimensional bodies at high angles of attack, and desirable and undesirable cross-sectional shapes, as determined from the two-dimensional tests, are indicated. The results are particularly applicable to spin characteristics since the high angles of attack often encountered minimize the axial-flow effect, and the results also indicate that, for certain cross sections, care must be exercised in using test results obtained at low Reynolds numbers to predict full-scale spin-recovery characteristics.

Langley Aeronautical Laboratory,
National Advisory Committee for Aeronautics,
Langley Field, Va., September 17, 1957.

REFERENCES

1. Letko, William, and Williams, James L.: Experimental Investigation at Low Speed of Effects of Fuselage Cross Section on Static Longitudinal and Lateral Stability Characteristics of Models Having 0° and 45° Sweptback Surfaces. NACA TN 3551, 1955.

2. Irving, H. B., Batson, A. S., and Warsap, J. H.: The Contribution of the Body and Tail of an Aeroplane to the Yawing Moment in a Spin. R. & M. No. 1689, British A.R.C., 1936.

3. Allen, H. Julian, and Perkins, Edward W.: A Study of Effects of Viscosity on Flow Over Slender Inclined Bodies of Revolution. NACA Rep. 1048, 1951. (Supersedes NACA TN 2044.)

4. Kelly, Howard R.: The Estimation of Normal-Force, Drag, and Pitching-Moment Coefficients for Blunt-Based Bodies of Revolution at Large Angles of Attack. Jour. Aero. Sci., vol. 21, no. 8, Aug. 1954, pp. 549-555, 565.

5. Bursnall, William J., and Loftin, Laurence K., Jr.: Experimental Investigation of the Pressure Distribution About a Yawed Circular Cylinder in the Critical Reynolds Number Range. NACA TN 2463, 1951.

6. Delany, Noel K., and Sorensen, Norman E.: Low-Speed Drag of Cylinders of Various Shapes. NACA TN 3038, 1953.

7. Lindsey, W. F.: Drag of Cylinders of Simple Shapes. NACA Rep. 619, 1938.

8. Zahm, A. F., Smith, R. H., and Louden, F. A.: Forces on Elliptic Cylinders in Uniform Air Stream. NACA Rep. 289, 1928.

9. Allen, H. Julian, and Vincenti, Walter G.: Wall Interference in a Two-Dimensional-Flow Wind Tunnel, With Consideration of the Effect of Compressibility. NACA Rep. 782, 1944. (Supersedes NACA WR A-63.)

10. Wieselsberger, C.: New Data on the Laws of Fluid Resistance. NACA TN 84, 1922.

11. Stack, John: Compressibility Effects in Aeronautical Engineering. NACA ACR, Aug. 1941.

12. Maruhn, K.: Aerodynamische Untersuchungen an Rümpfen mit rechteckähnlichem Querschnitt. Jahrb. 1942 der deutschen Luftfahrtforschung, R. Oldenbourg (Munich), I 263 - I 279.

13. Wieselsberger, C.: Versuche über den Luftwiderstand gerundeter und kantiger Körper. (c) Der Widerstand verschiedener Körper. Ergb. Aerod. Versuchsanstalt zu Göttingen, Lfg. II, R. Oldenbourg (Munich), 1923, pp. 33-35.

14. Jacobs, Eastman N., and Sherman, Albert.: Airfoil Section Characteristics As Affected by Variations of the Reynolds Number. NACA Rep. 586, 1937.

15. Perkins, Edward W., and Jorgensen, Leland H.: Comparison of Experimental and Theoretical Normal-Force Distributions (Including Reynolds Number Effects) on an Ogive-Cylinder Body at Mach Number 1.98. NACA TN 3716, 1956. (Supersedes NACA RM A54H23.)

TABLE I

DETAILS OF FUSELAGES TESTED

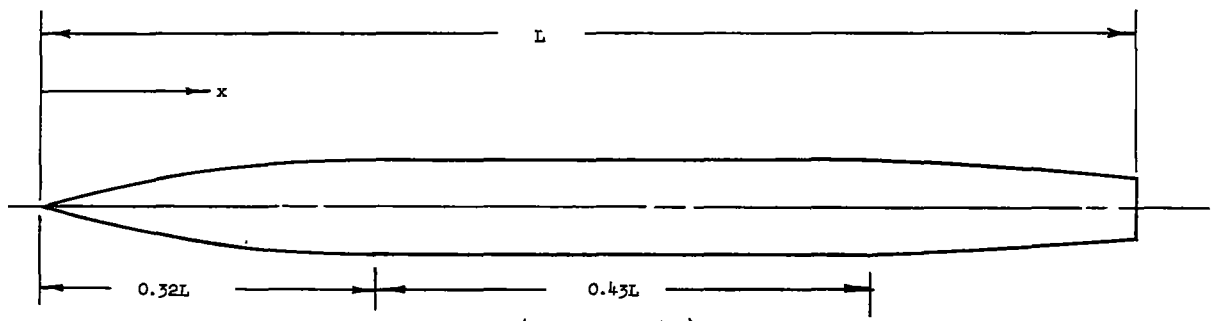

(Constant section)

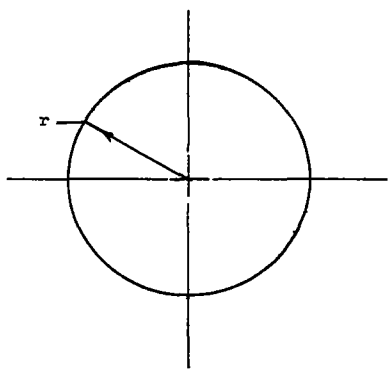

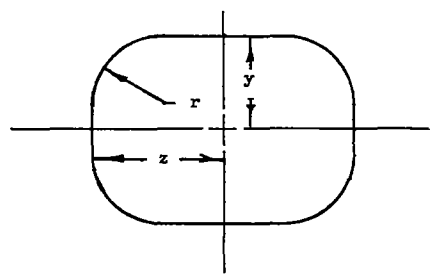

Coordinates for circular fuselage	
x/L	r/L
0	0
.0328	.0091
.0657	.0171
.0986	.0241
.1315	.0300
.1643	.0350
.1972	.0390
.2301	.0421
.2629	.0443
.2958	.0453
.3200	.0457
.7534	.0457
.7669	.0454
.7998	.0438
.8326	.0418
.8655	.0395
.8984	.0372
.9313	.0349
.9641	.0326
1.0000	.0302

Coordinates for rectangular fuselages			
x/L	y/L	z/L	r/L
0	0	0	0
.0219	.0059	.0062	.0056
.0657	.0149	.0173	.0127
.0877	.0186	.0230	.0150
.1315	.0242	.0321	.0179
.1534	.0265	.0362	.0188
.1972	.0300	.0427	.0198
.2410	.0323	.0475	.0202
.2630	.0331	.0492	.0203
.2849	.0336	.0502	.0204
.3200	.0339	.0509	.0204
.7534	.0339	.0509	.0204
.7615	.0339	.0507	.0205
.7889	.0336	.0489	.0213
.8327	.0329	.0451	.0231
.8546	.0325	.0430	.0240
.8985	.0317	.0388	.0259
.9204	.0313	.0369	.0269
.9642	.0306	.0331	.0286
1.0000	.0301	.0301	.0301

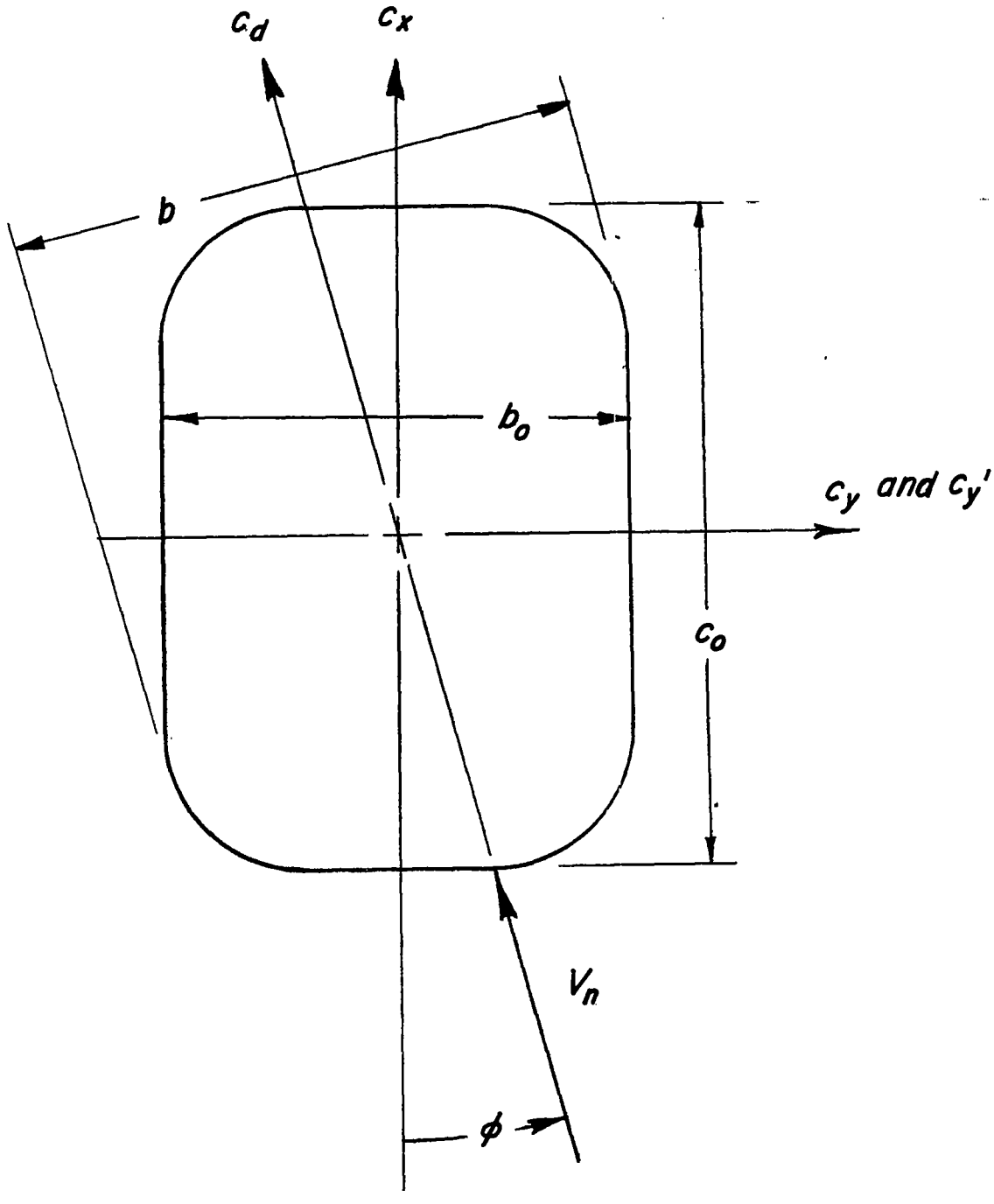

Figure 1.- Convention used to define positive sense of the flow inclination, cylinder reference dimensions, and aerodynamic coefficients.

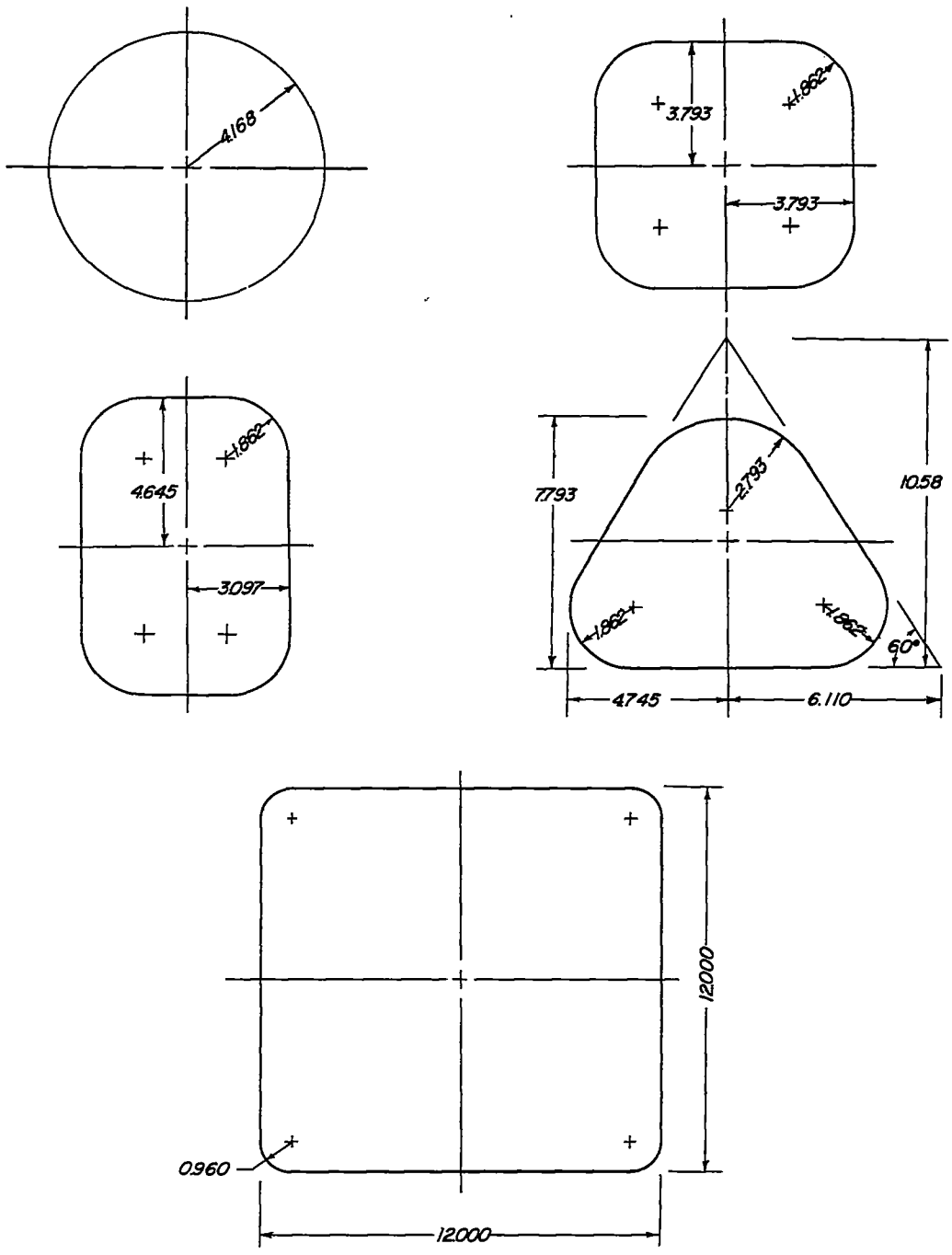

(a) Cross-sectional details. (Dimensions in inches.)

Figure 2.- Details of two-dimensional cylinders.

L-93699

(b) Photograph (taken from downstream side) of triangular cylinder mounted in wind tunnel.

Figure 2.- Concluded.

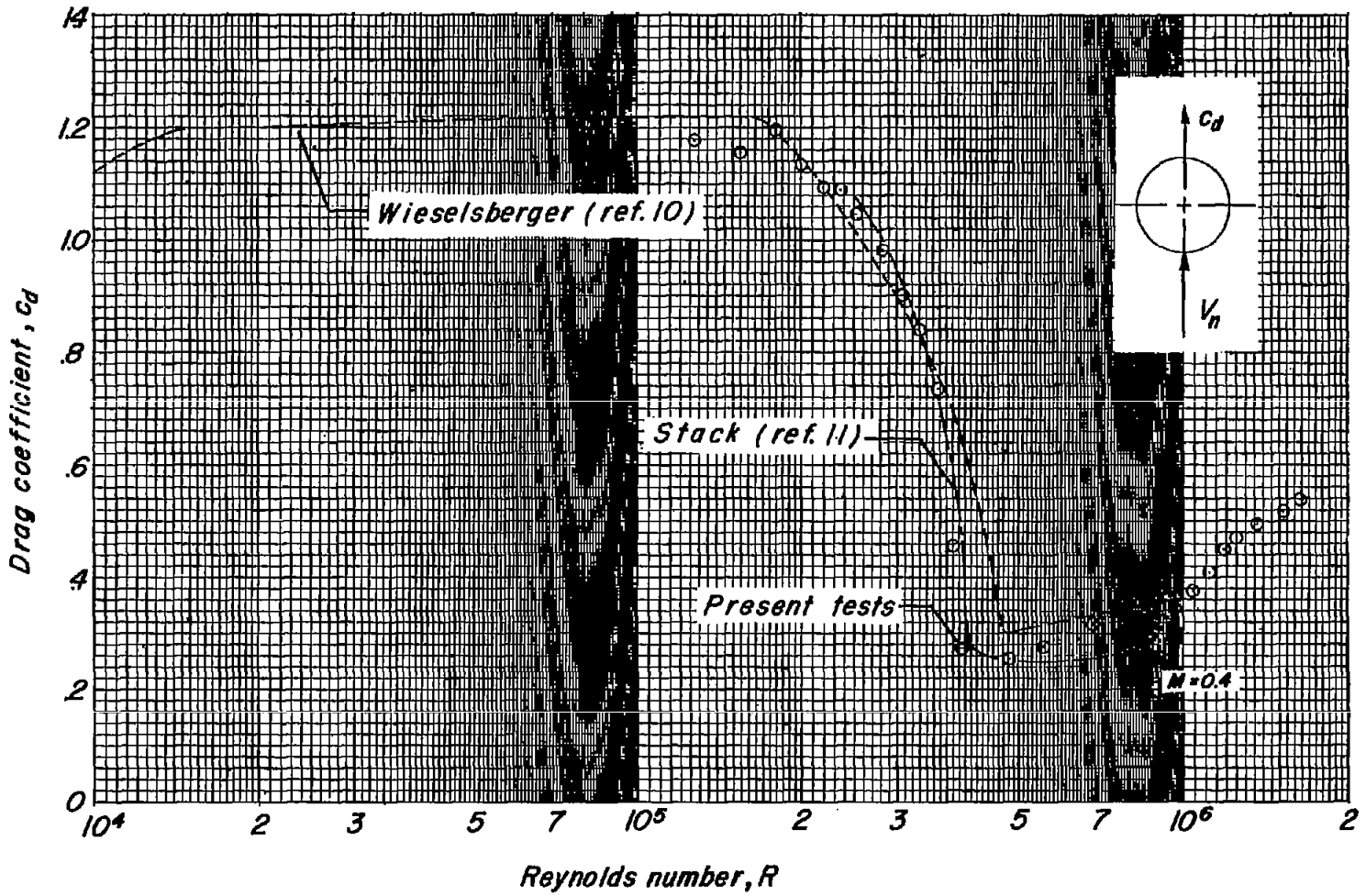

Figure 3.- Variation with Reynolds number of the drag coefficient of circular cylinders obtained by the present tests and compared with previous results.

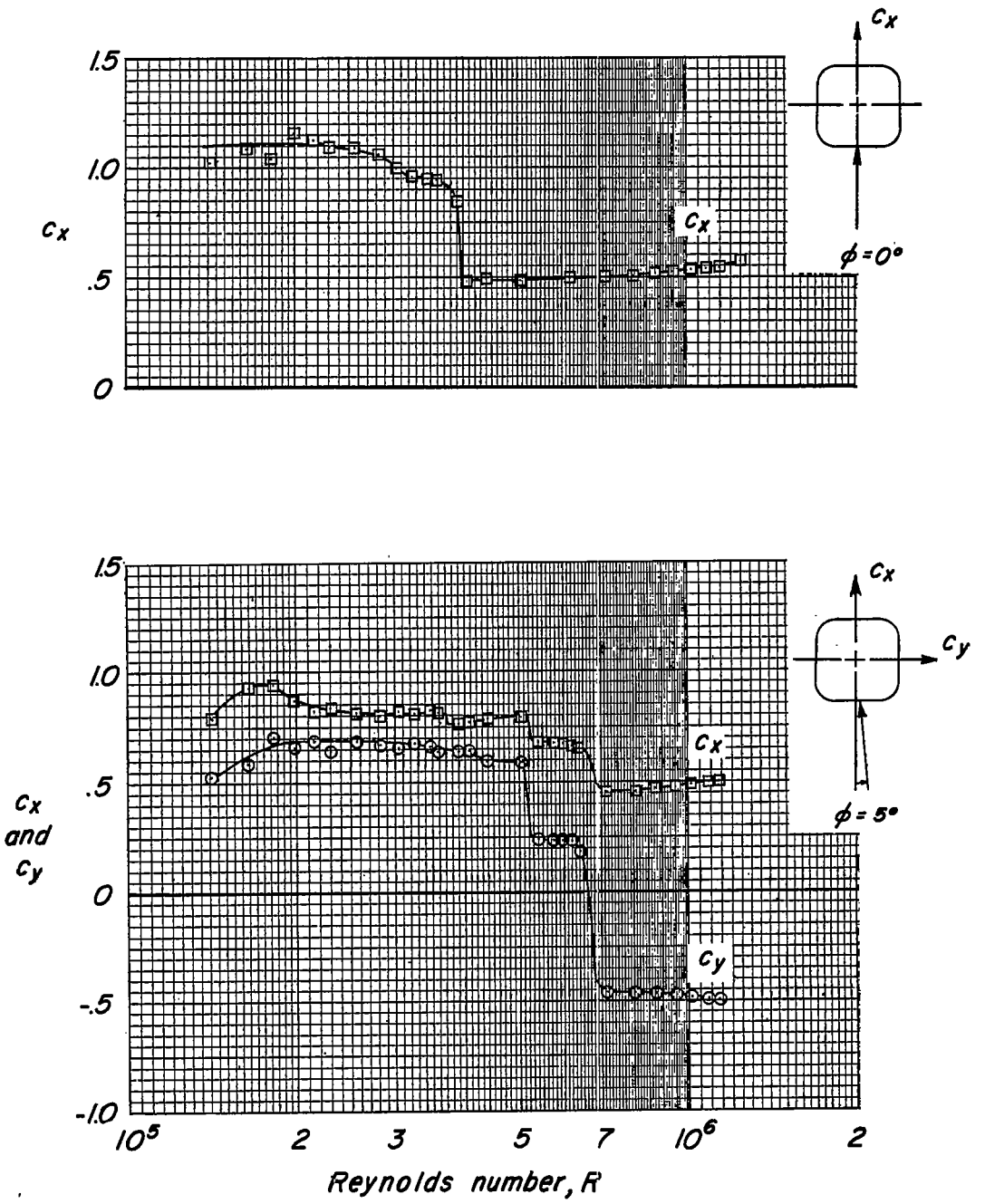

(a) $\phi = 0°$; $\phi = 5°$.

Figure 4.- Effect of Reynolds number on the force characteristics of a square cylinder. $r/b_o = 0.245$.

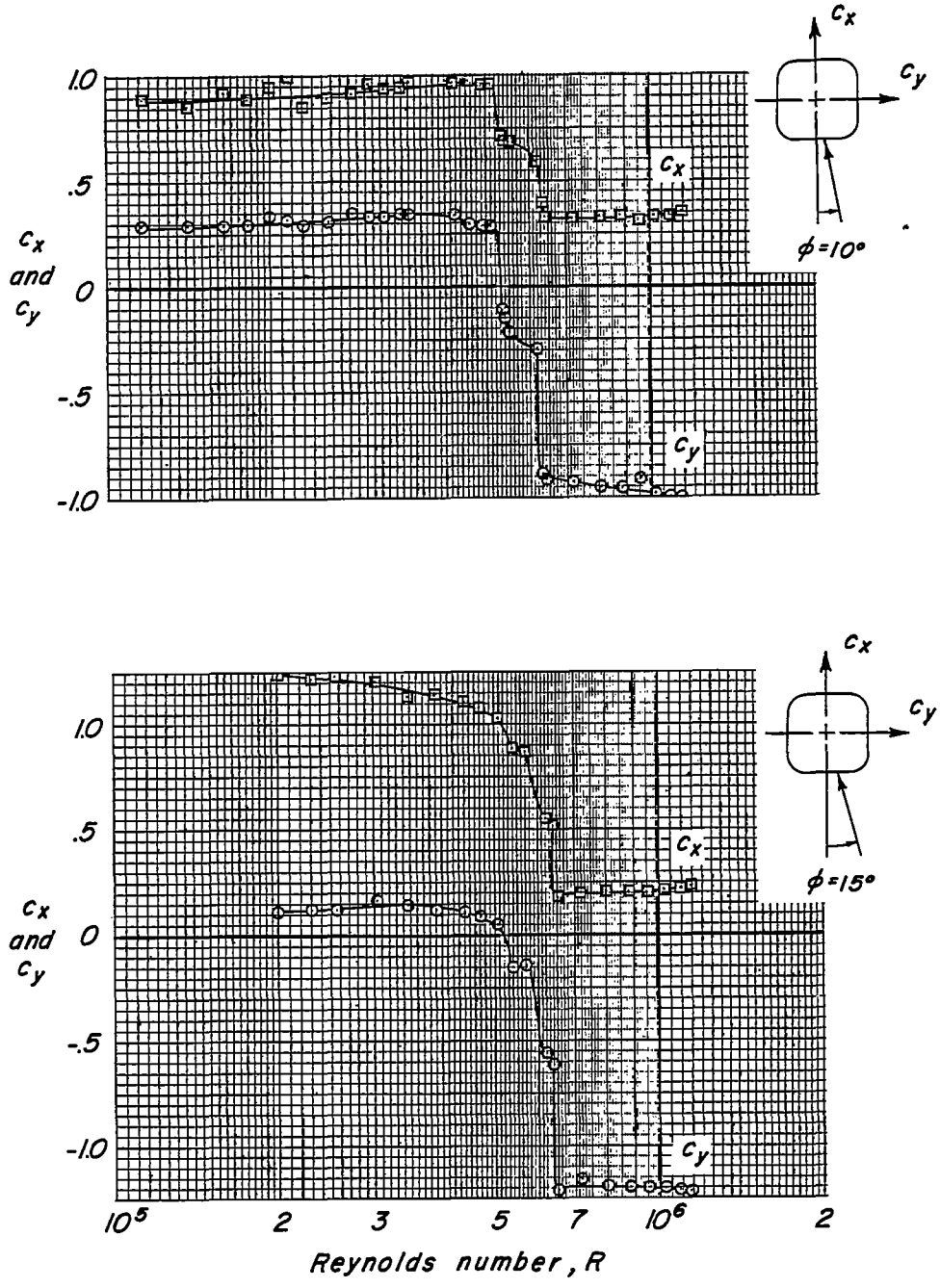

(b) $\phi = 10°$; $\phi = 15°$.

Figure 4.- Continued.

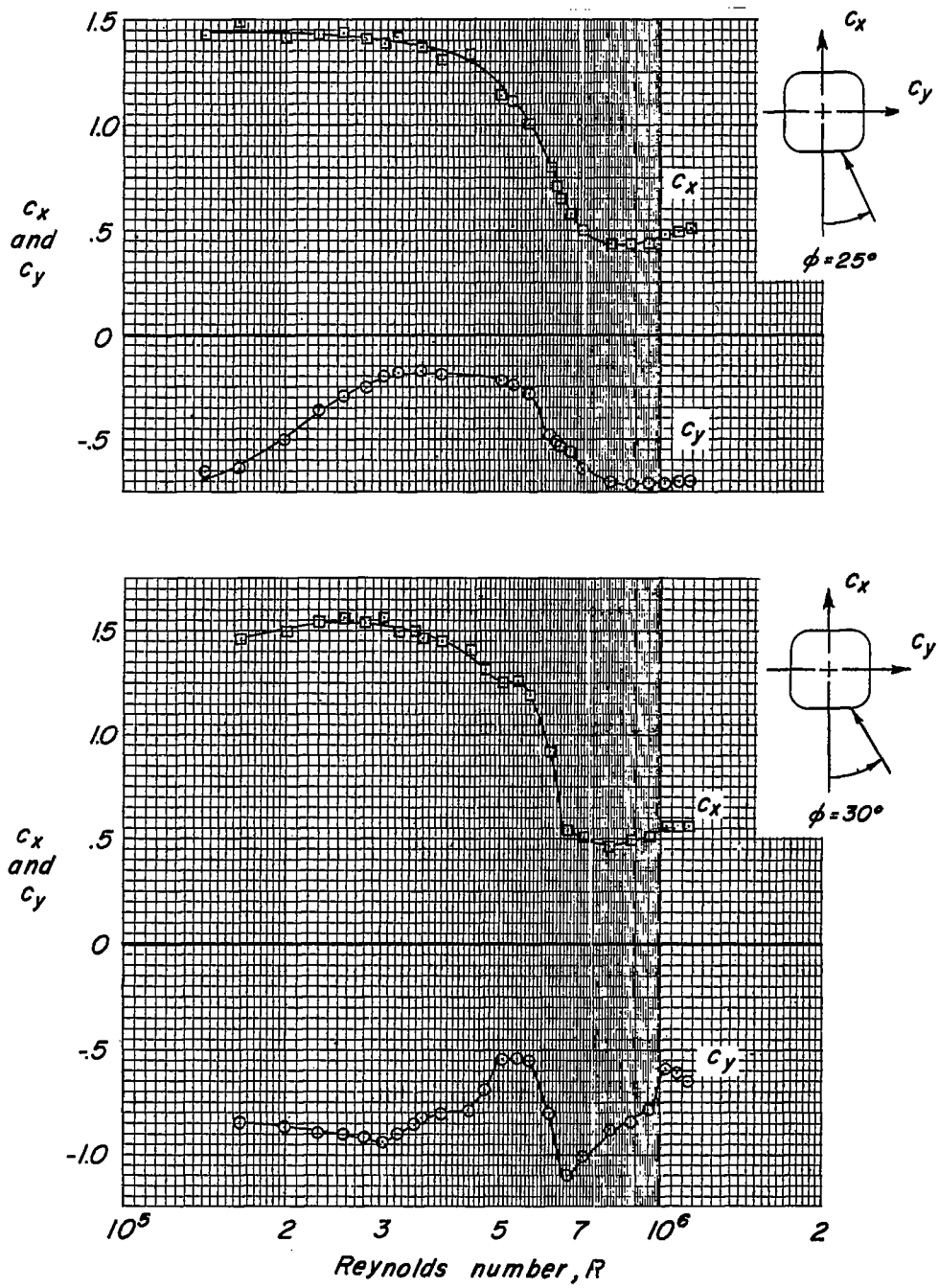

(c) $\phi = 25°$; $\phi = 30°$.

Figure 4.- Continued.

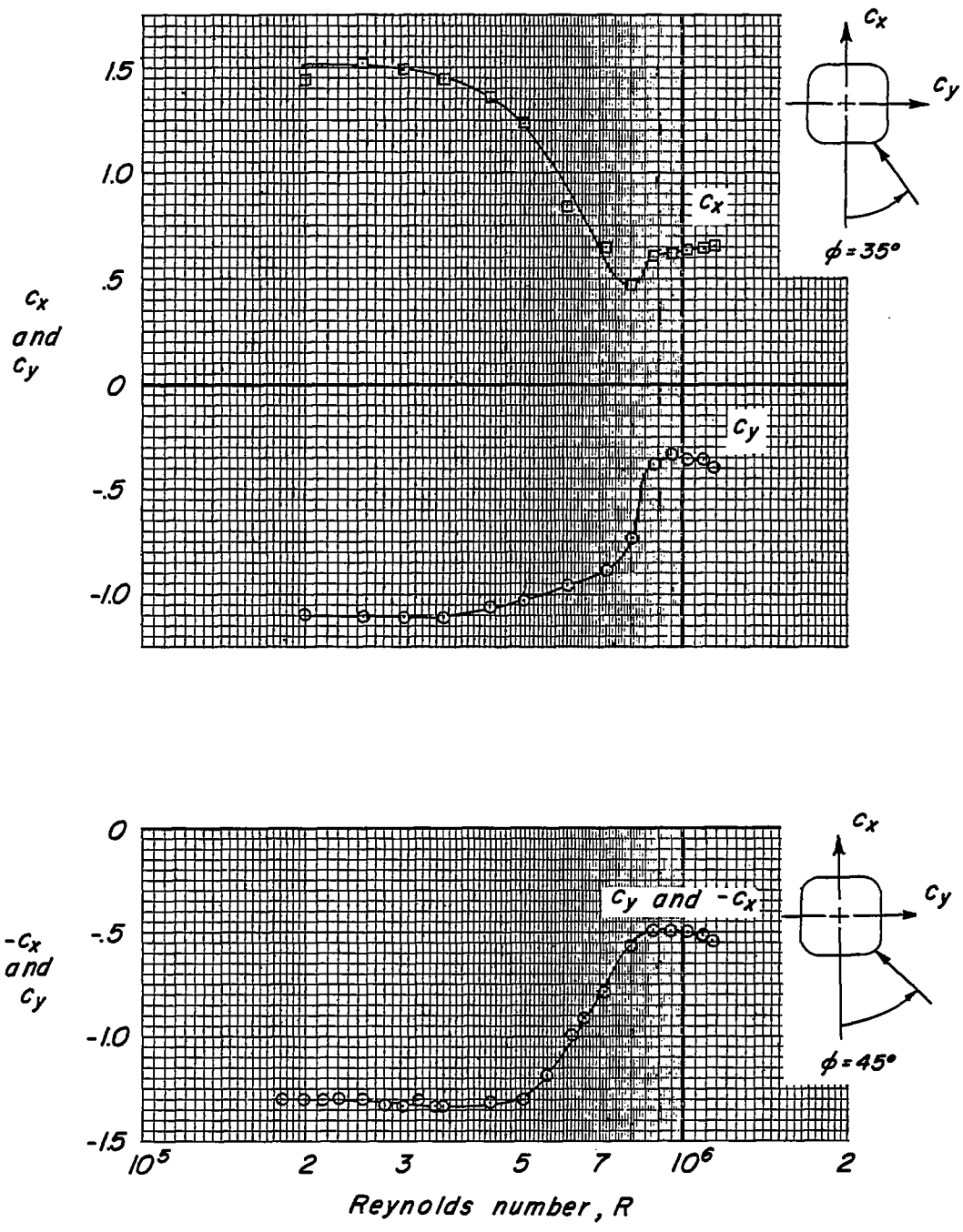

(d) $\phi = 35°$; $\phi = 45°$.

Figure 4.- Concluded.

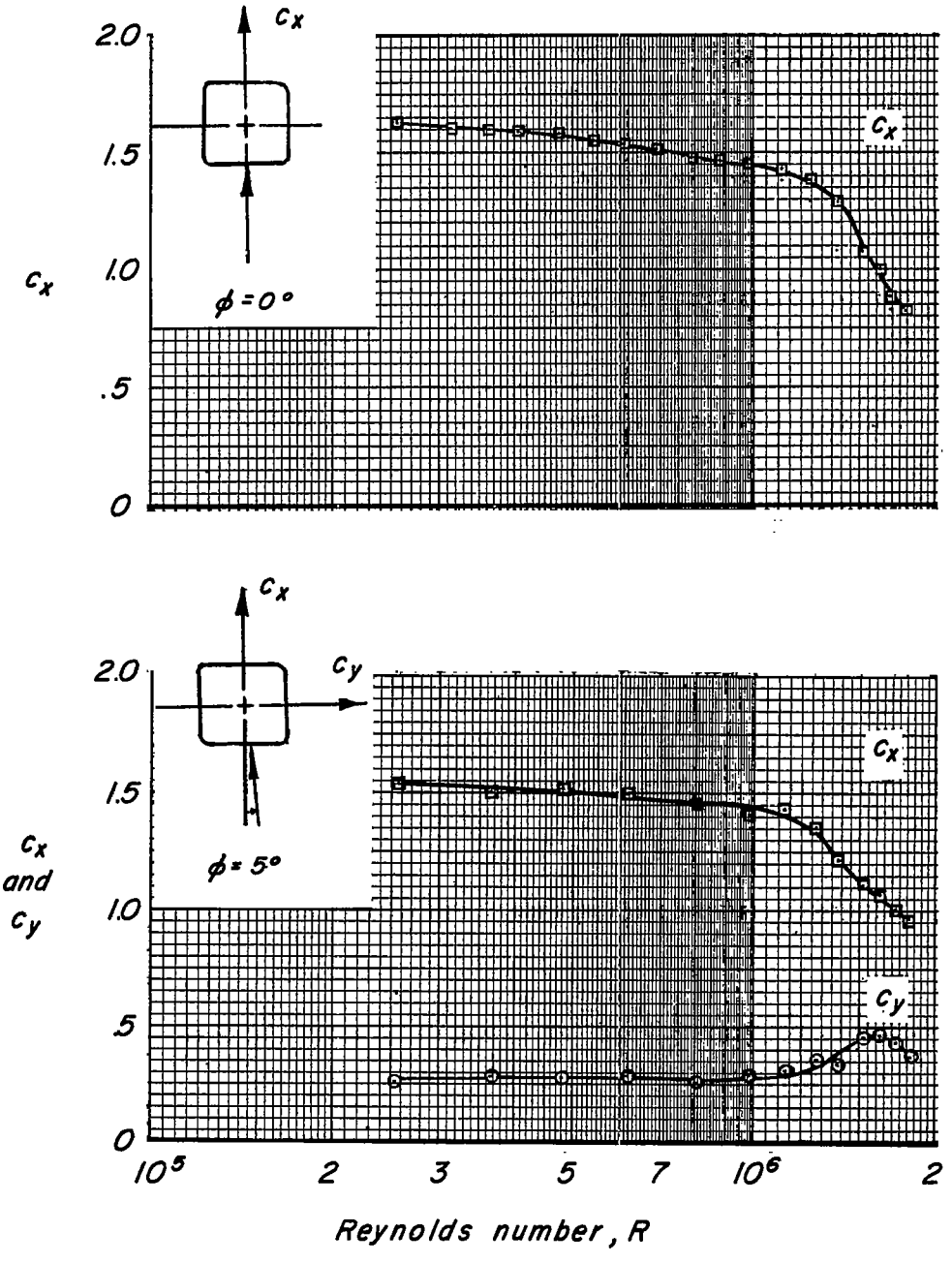

(a) $\phi = 0°$; $\phi = 5°$.

Figure 5.- Effect of Reynolds number on the force characteristics of a square cylinder. $r/b_o = 0.080$.

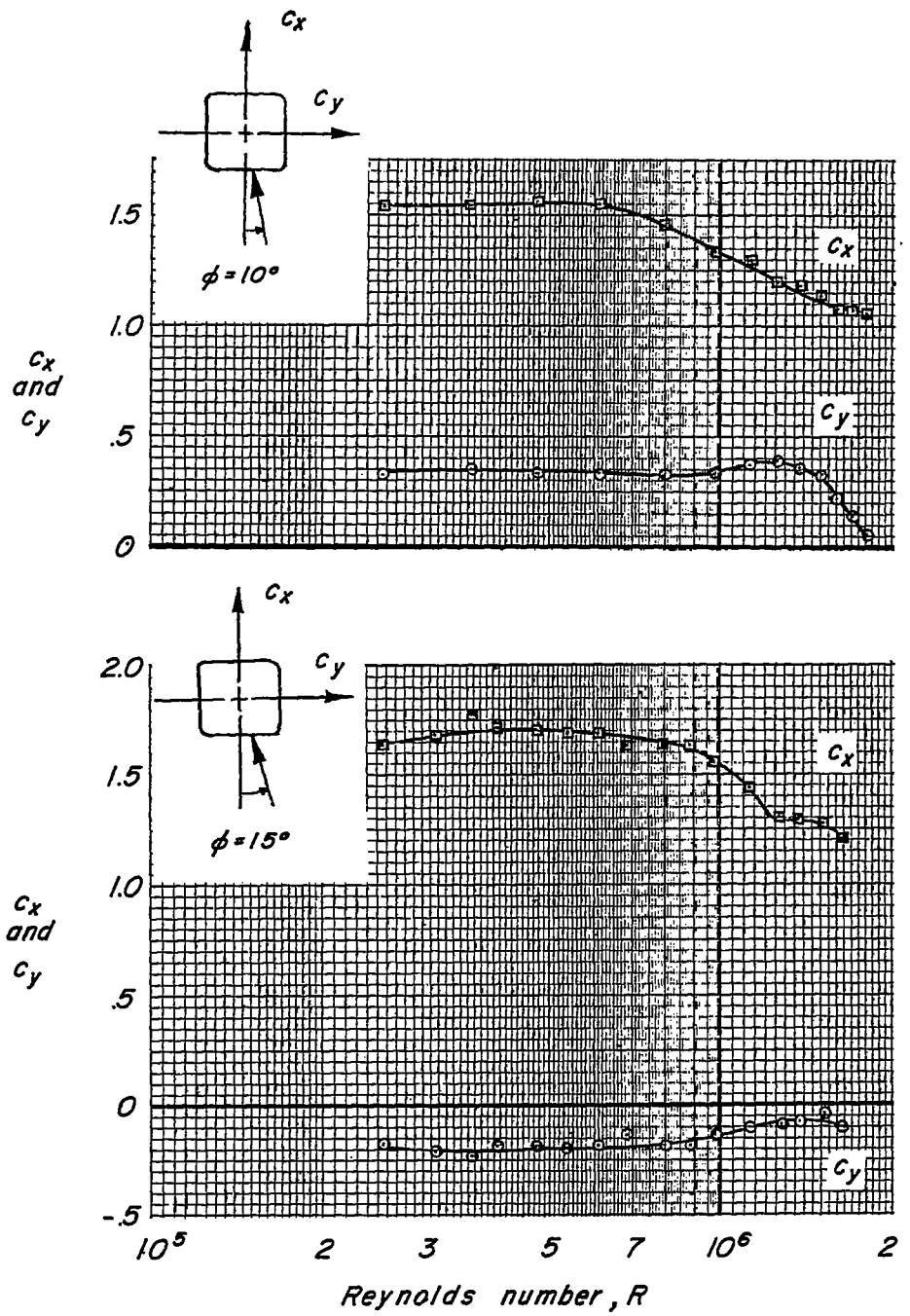

(b) $\phi = 10°$; $\phi = 15°$.

Figure 5.- Continued.

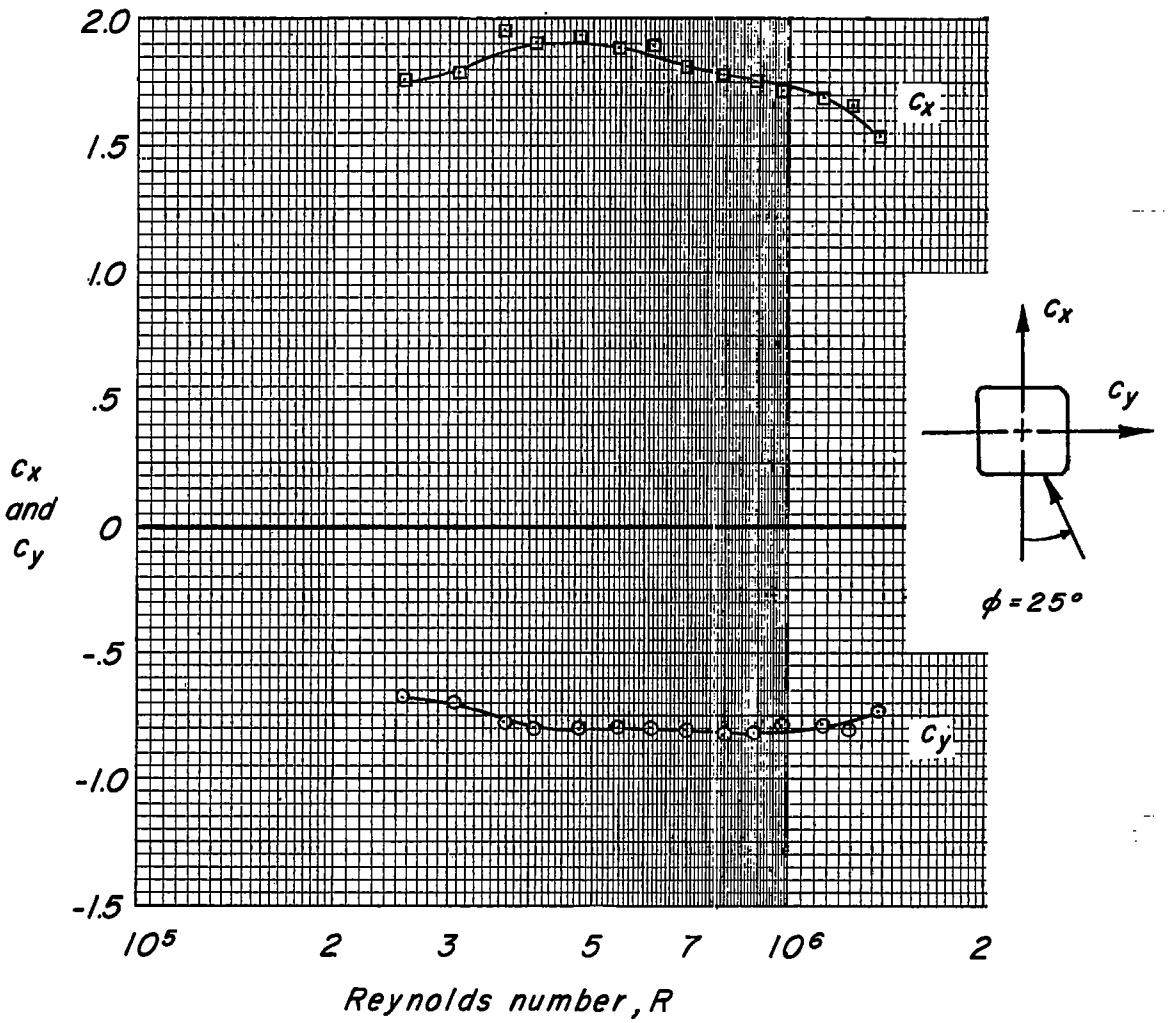

(c) $\phi = 25°$.

Figure 5.- Continued.

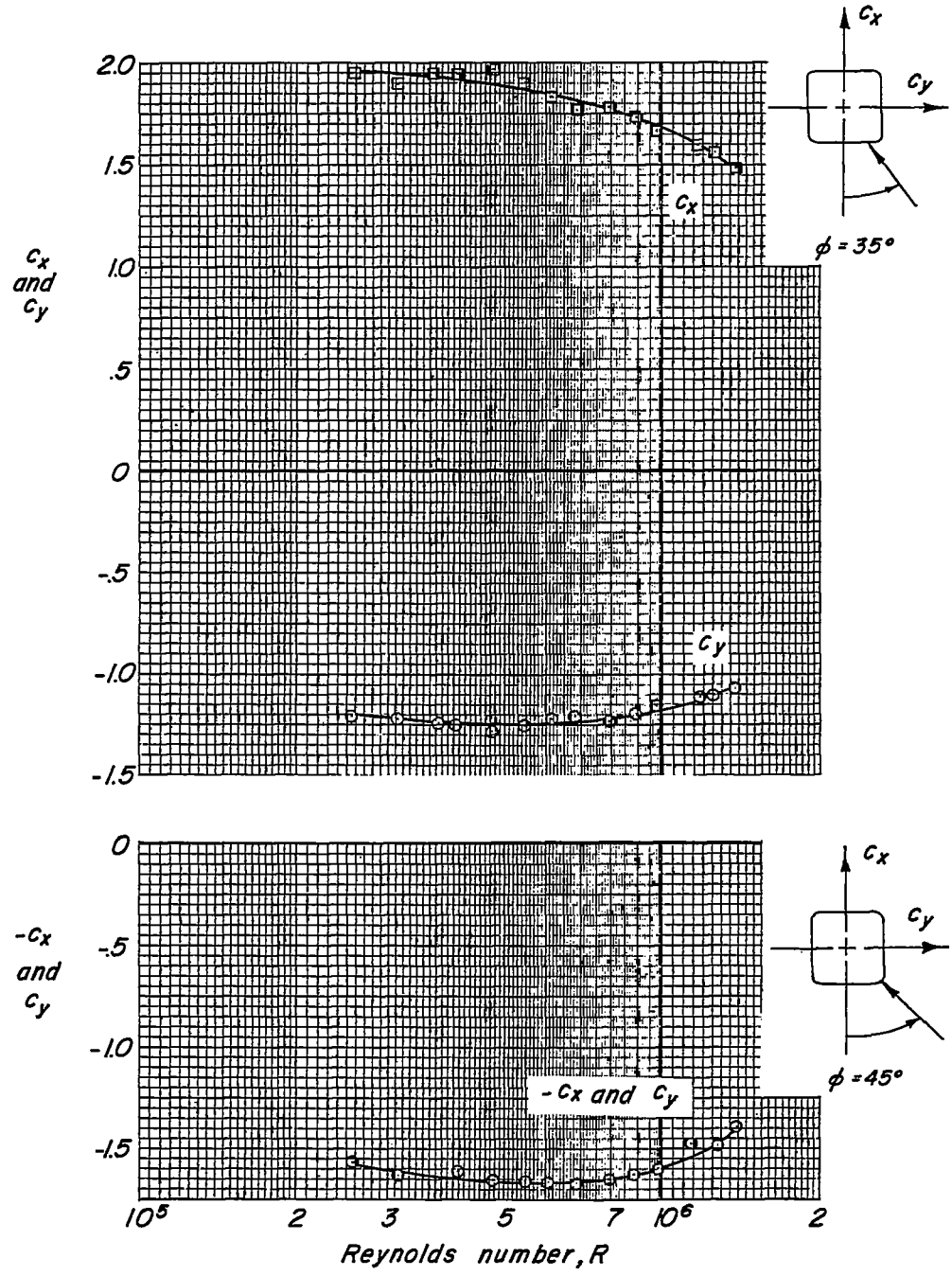

(d) $\phi = 35°$; $\phi = 45°$.

Figure 5.- Concluded.

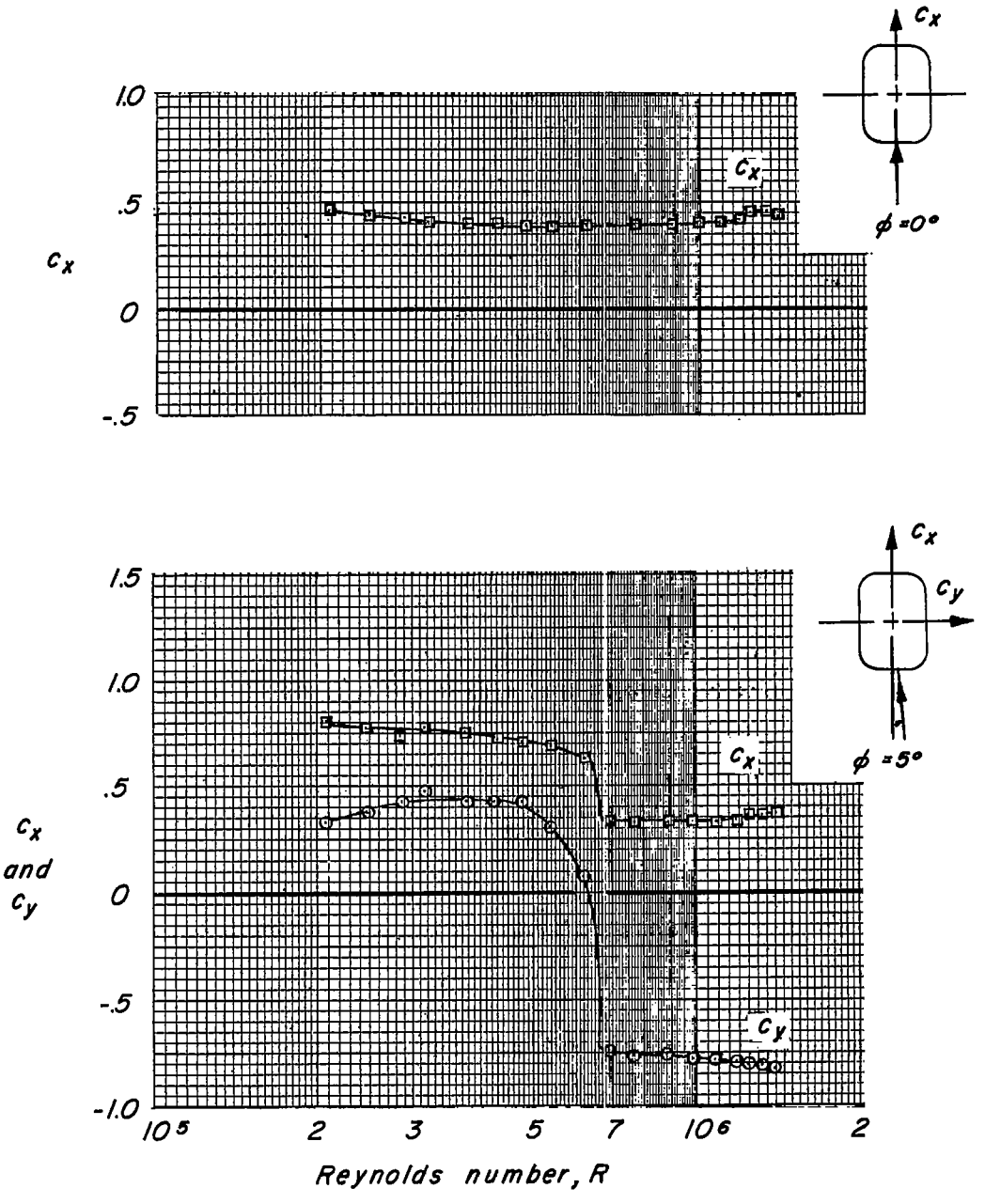

(a) $\phi = 0°$; $\phi = 5°$.

Figure 6.- Effect of Reynolds number on the force characteristics of a rectangular cylinder with its major axis parallel (at zero incidence) to the stream.

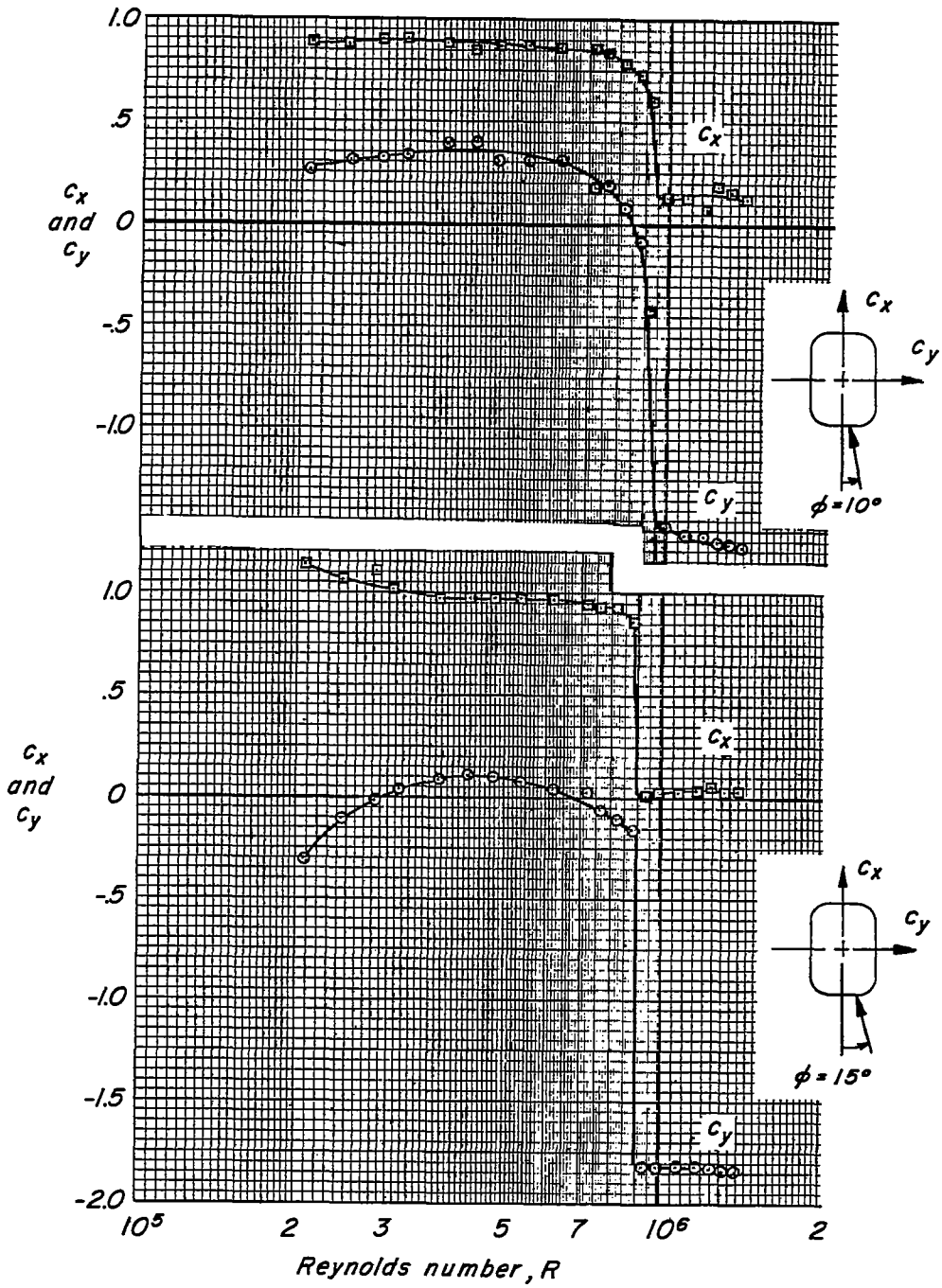

(b) $\phi = 10°$; $\phi = 15°$.

Figure 6.- Continued.

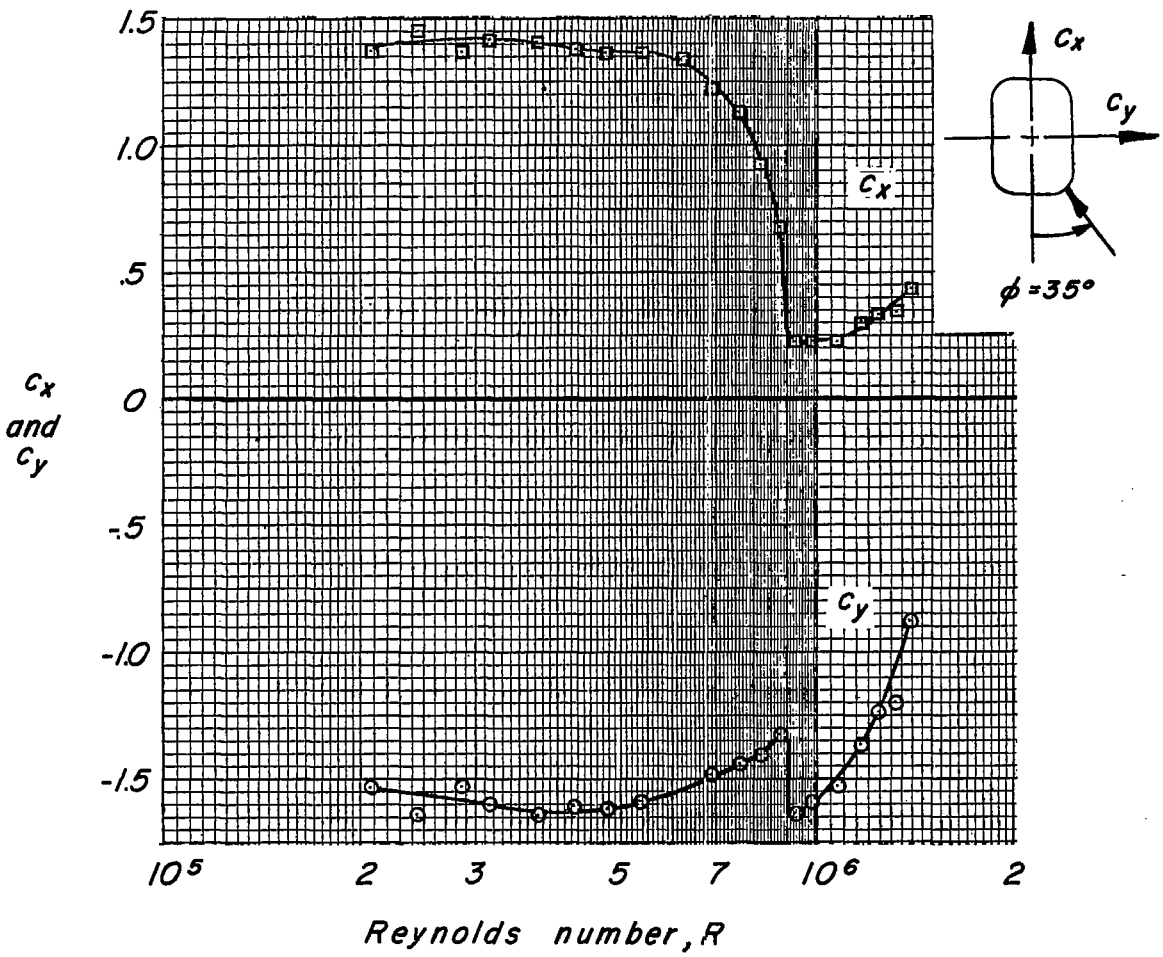

(c) $\phi = 35°$.

Figure 6.- Continued.

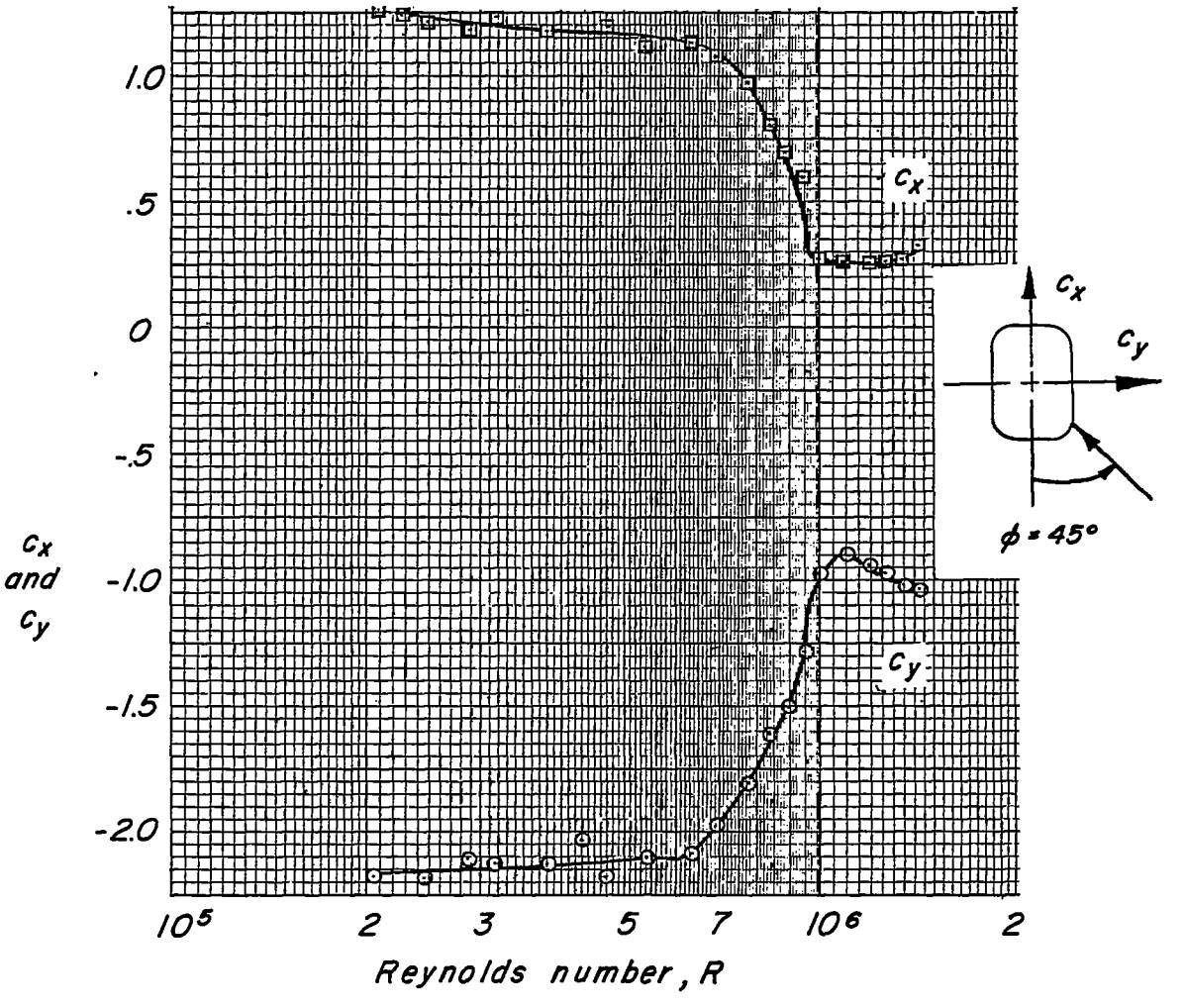

(d) $\phi = 45°$.

Figure 6.- Concluded.

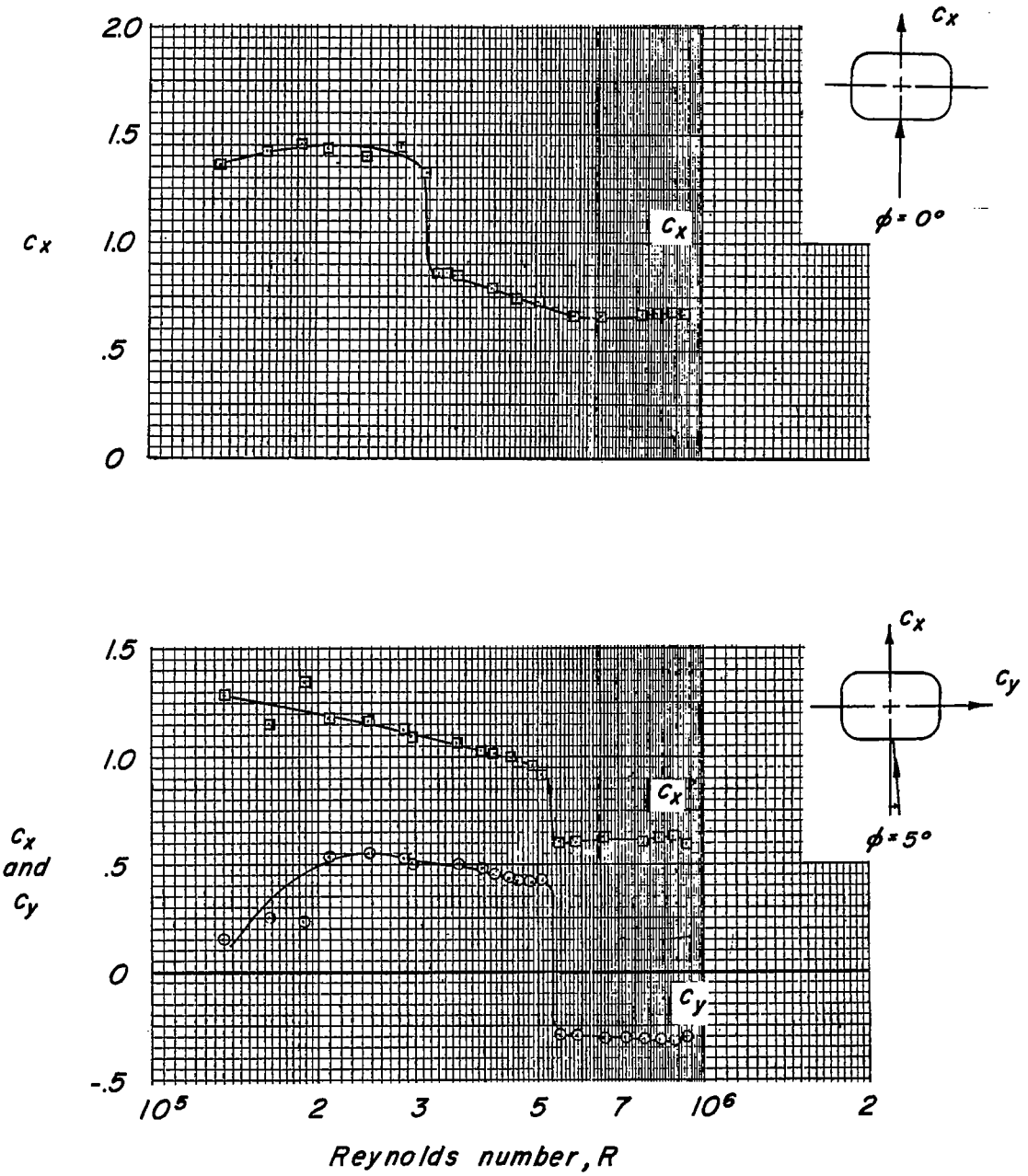

(a) $\phi = 0°$; $\phi = 5°$.

Figure 7.- Effect of Reynolds number on the force characteristics of a rectangular cylinder with its major axis normal (at zero incidence) to the stream.

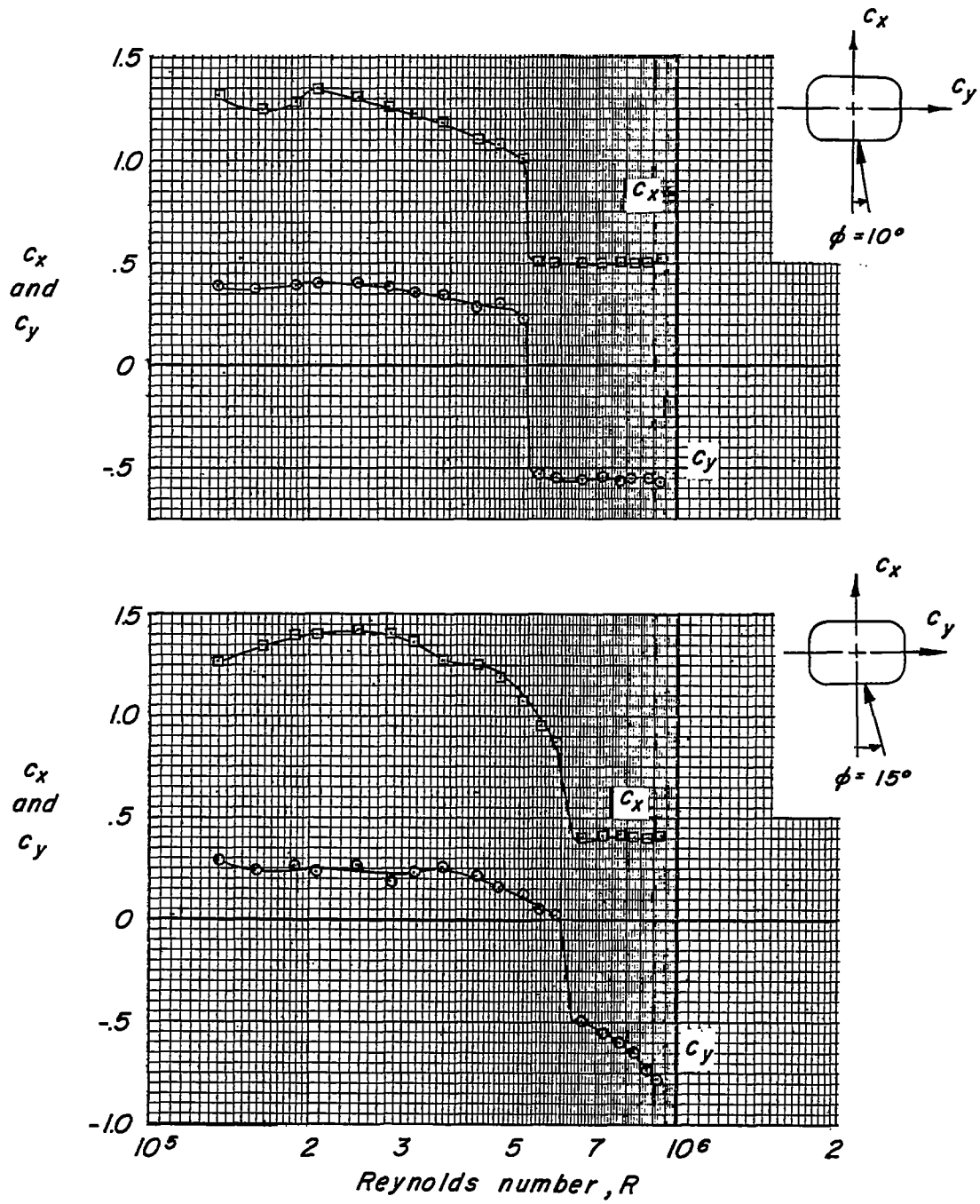

(b) $\phi = 10°$; $\phi = 15°$.

Figure 7.- Continued.

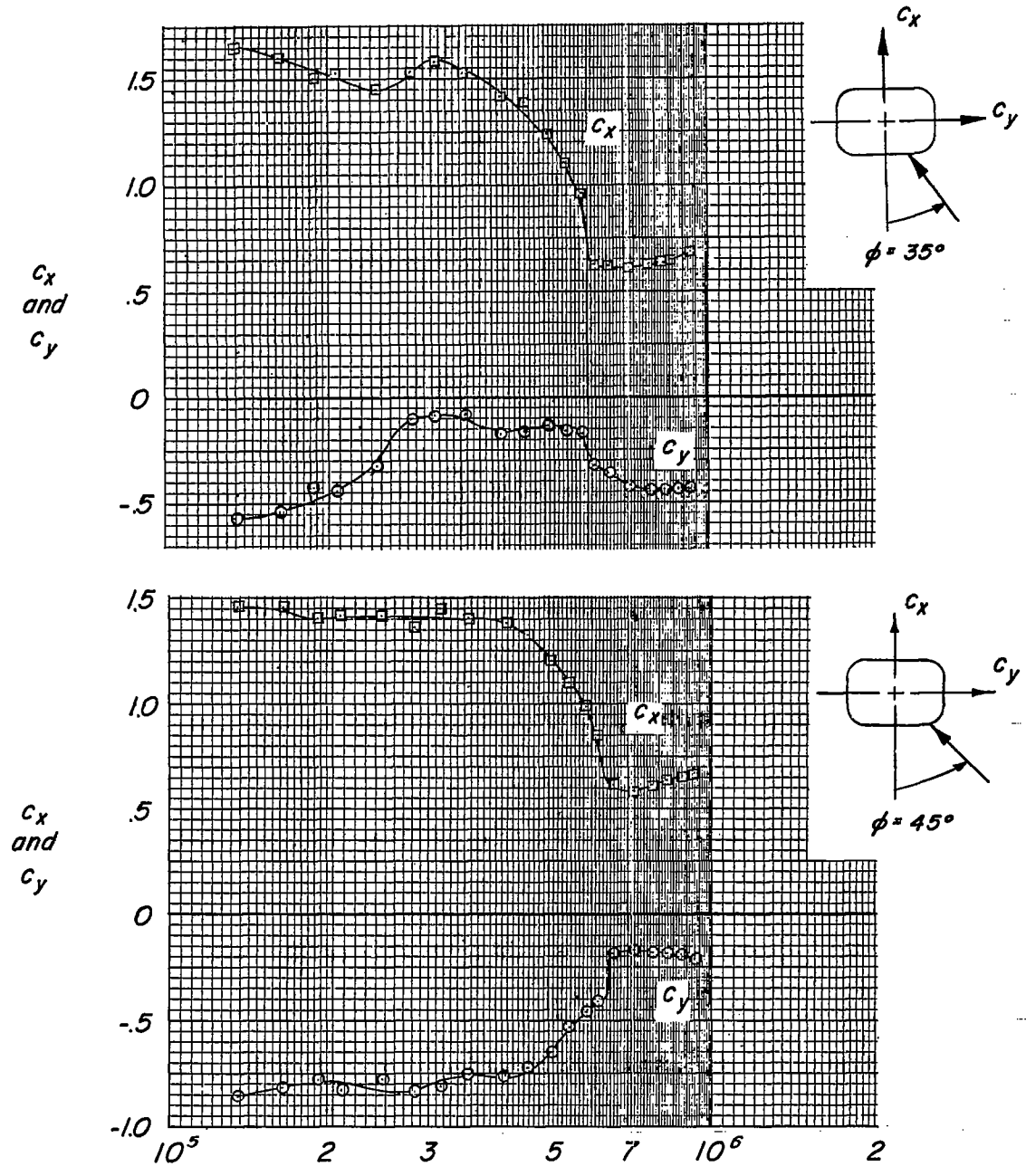

(c) $\phi = 35°$; $\phi = 45°$.

Figure 7.- Concluded.

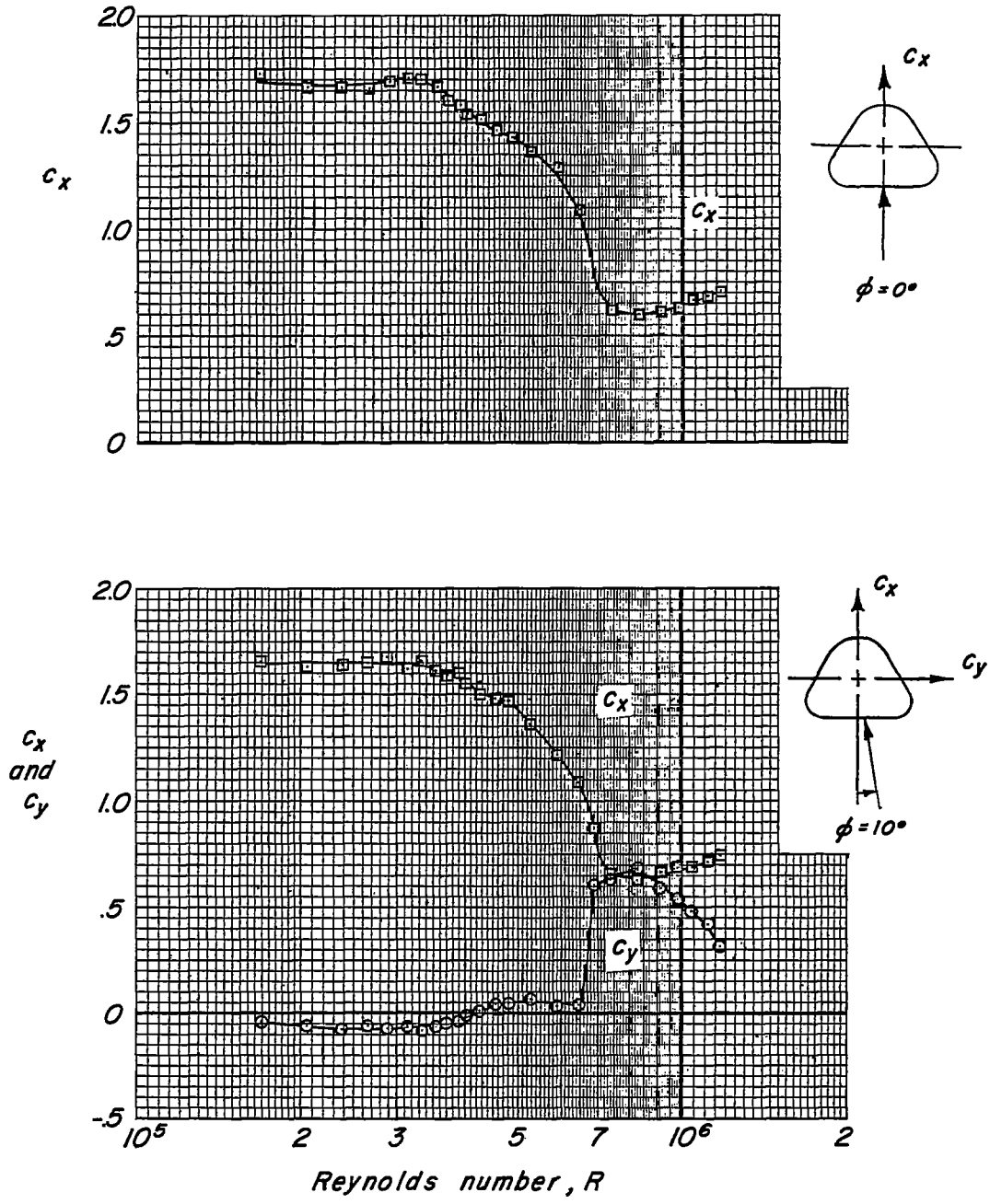

(a) $\phi = 0°$; $\phi = 10°$.

Figure 8.- Effect of Reynolds number on the force characteristics of the triangular cylinder.

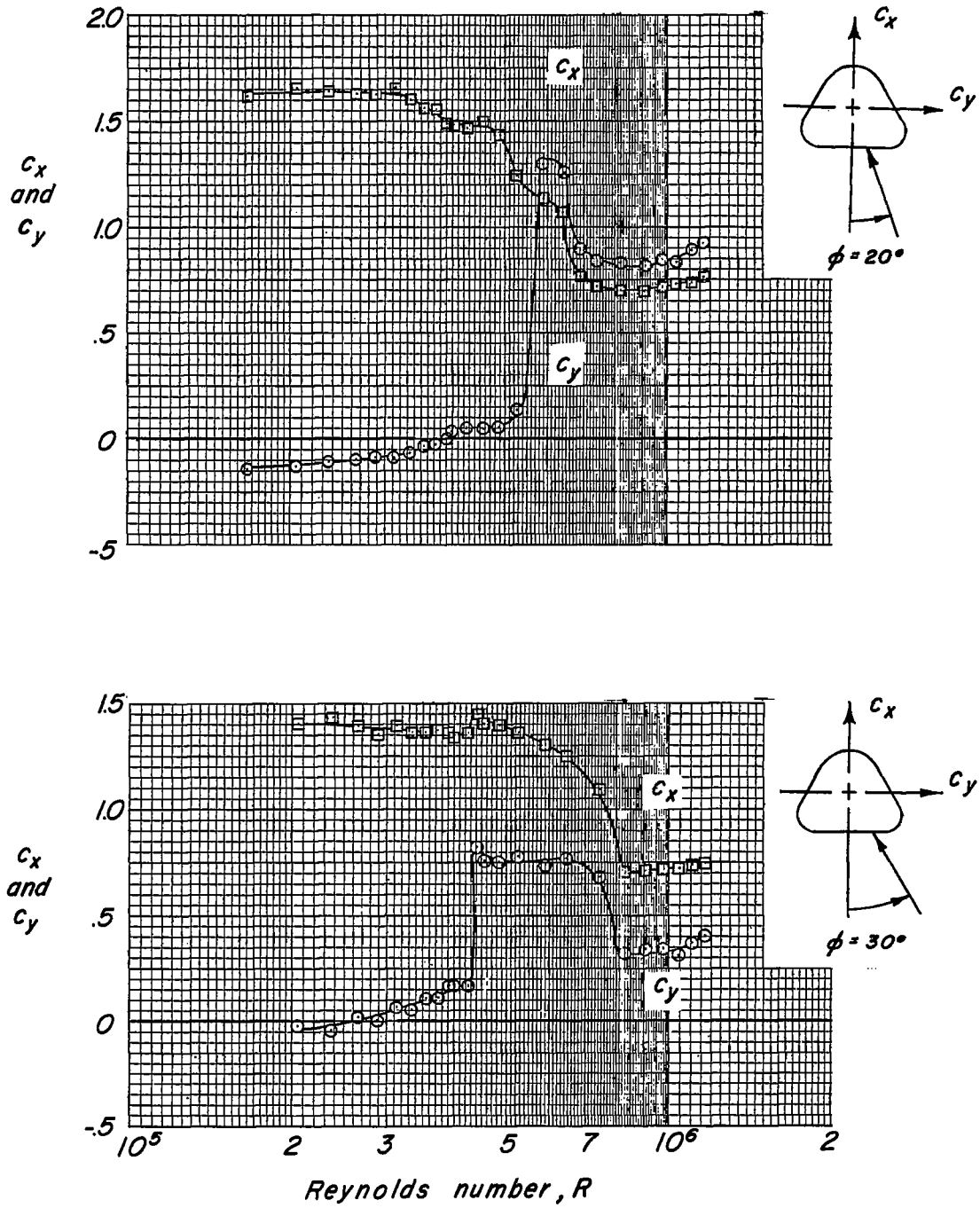

(b) $\phi = 20°$; $\phi = 30°$.

Figure 8.- Continued.

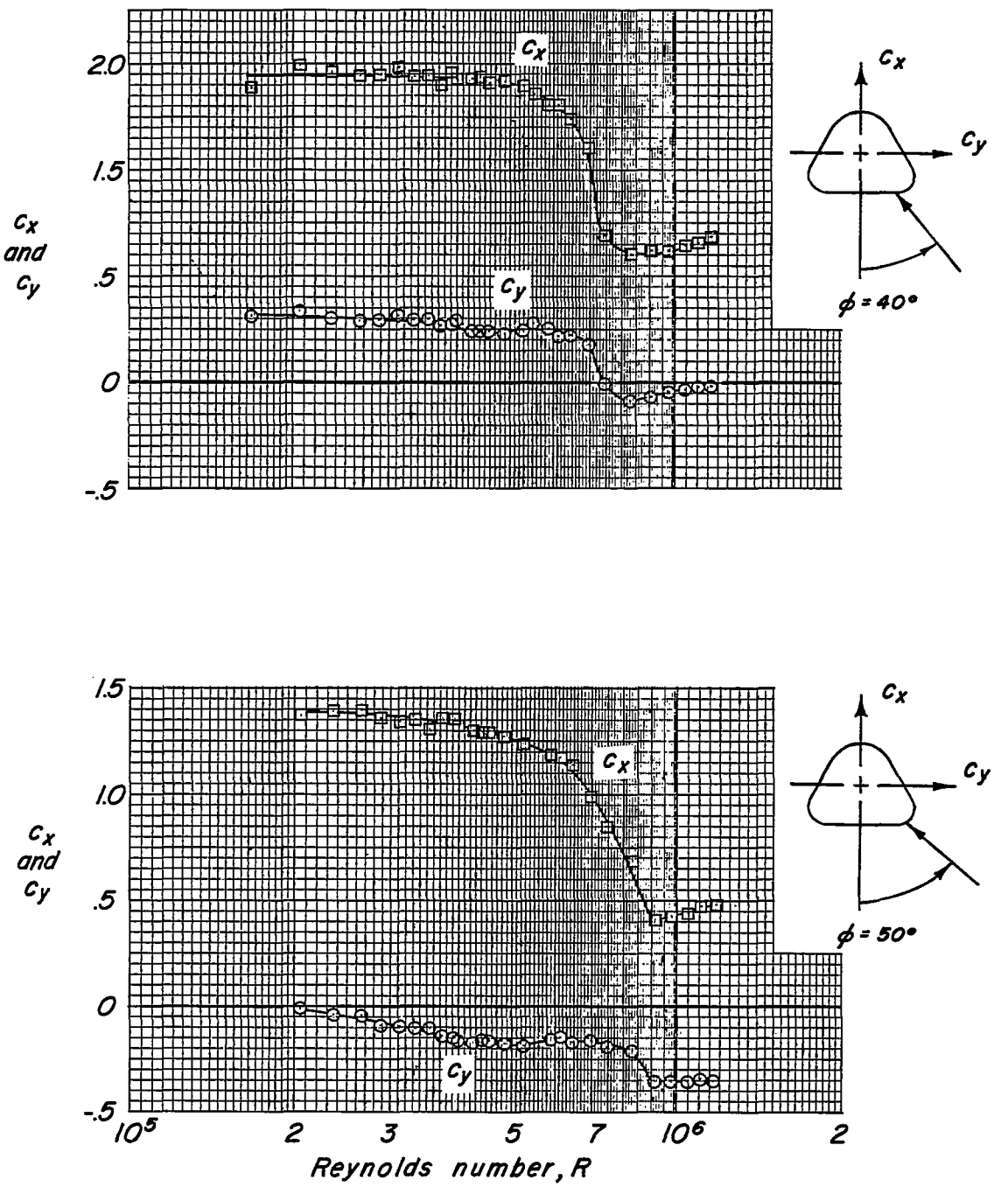

(c) $\phi = 40°$; $\phi = 50°$.

Figure 8.- Continued.

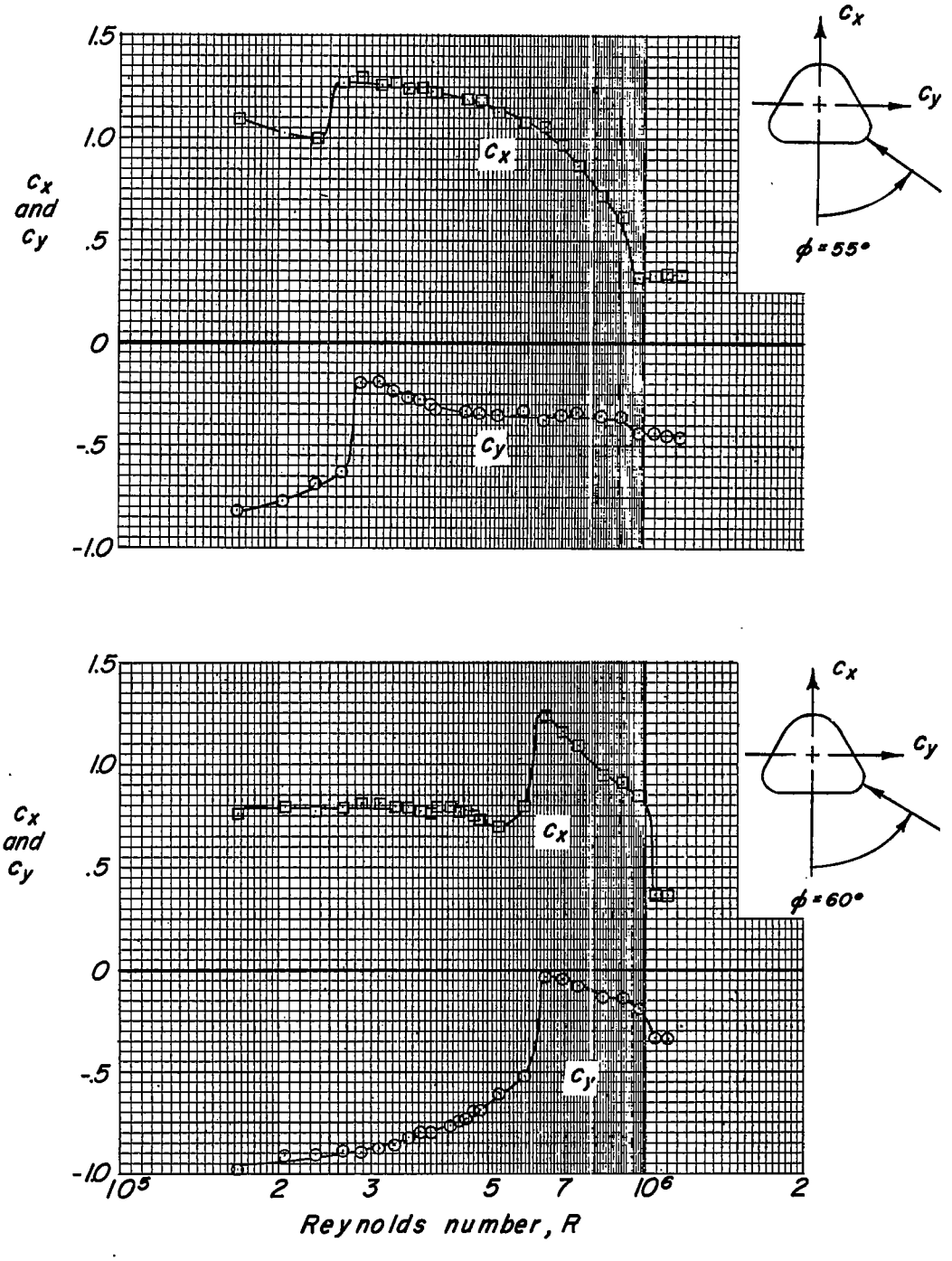

(d) $\phi = 55°$; $\phi = 60°$.

Figure 8.- Continued.

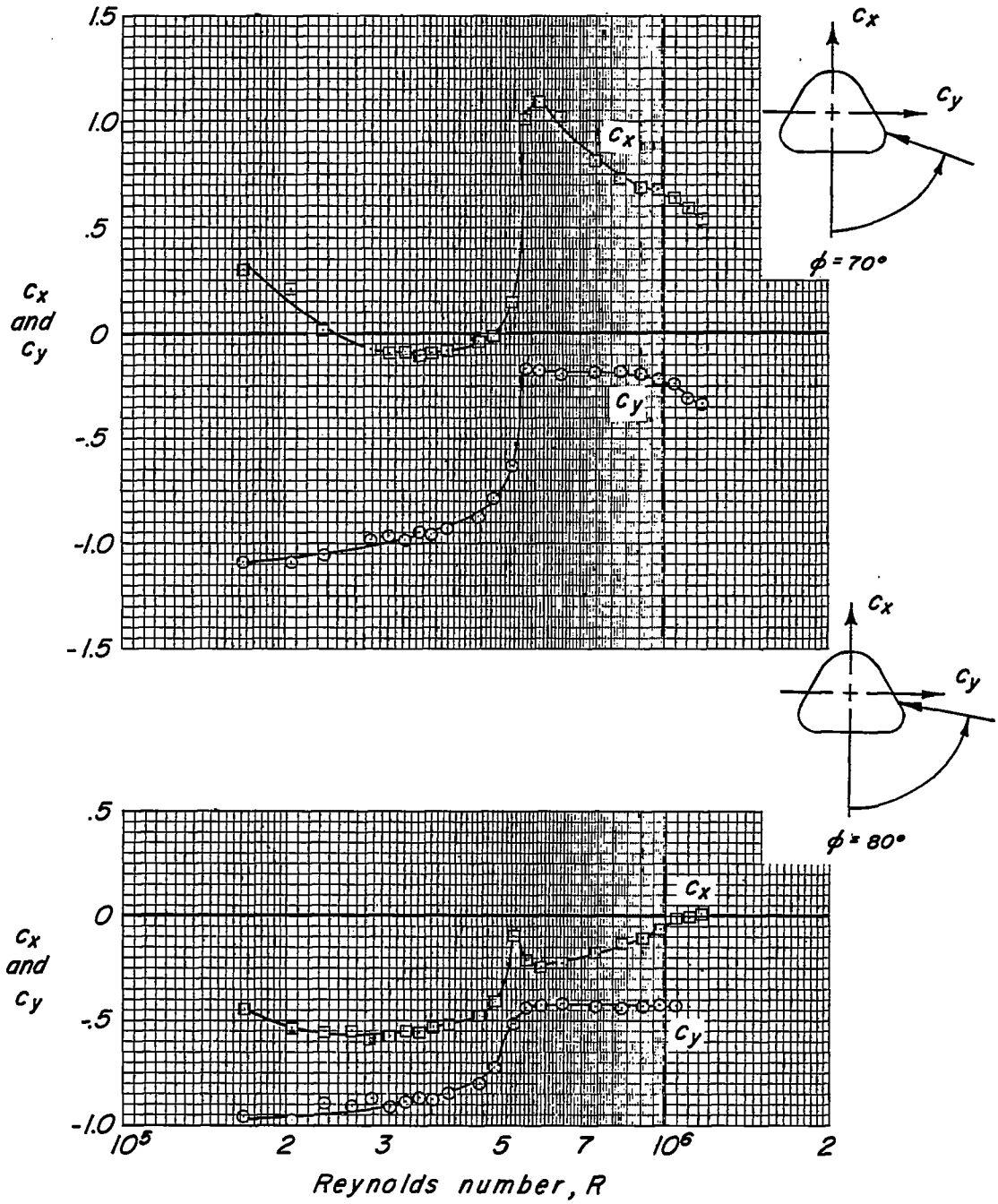

(e) $\phi = 70°$; $\phi = 80°$.

Figure 8.- Continued.

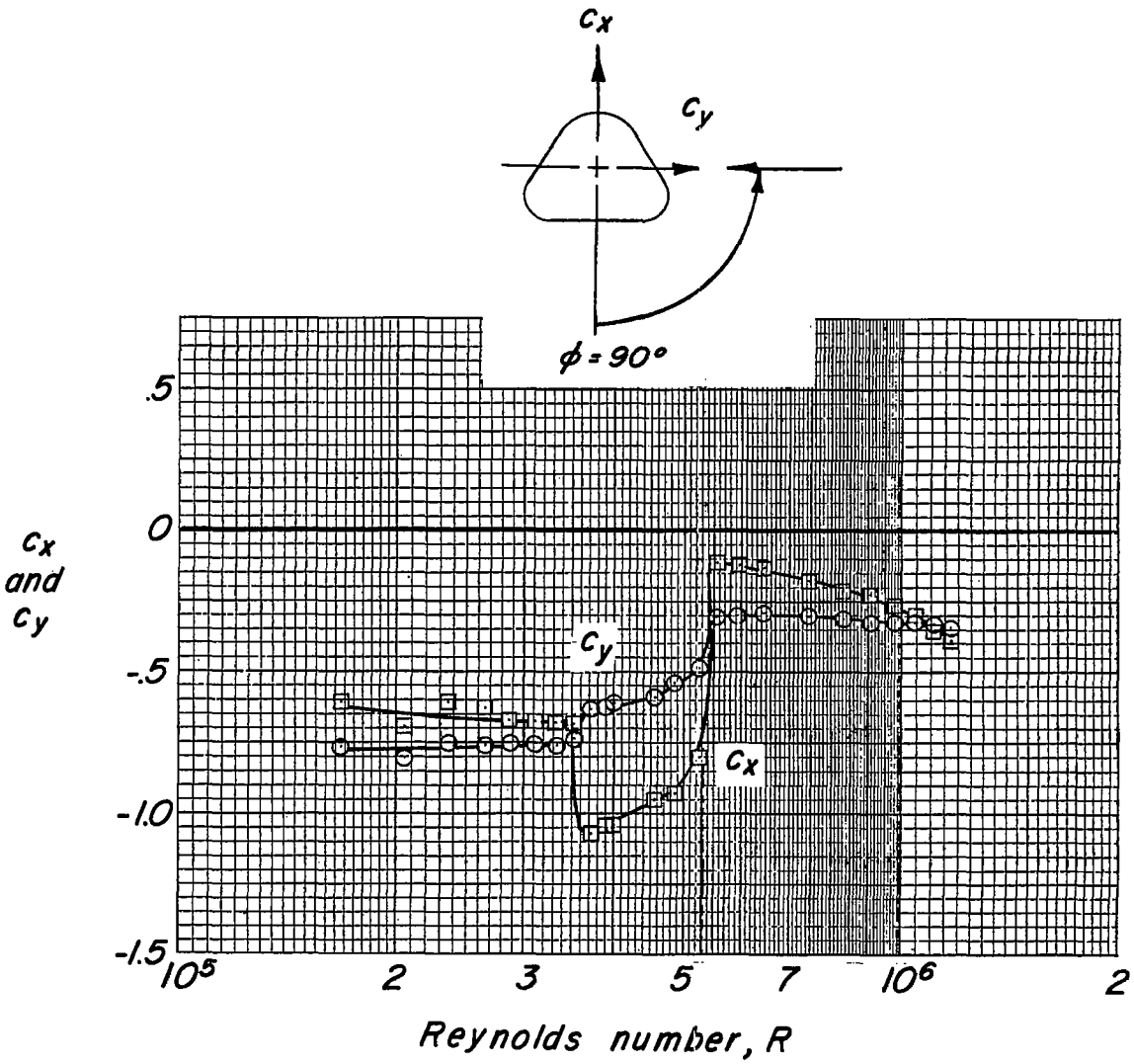

(f) $\phi = 90°$.

Figure 8.- Concluded.

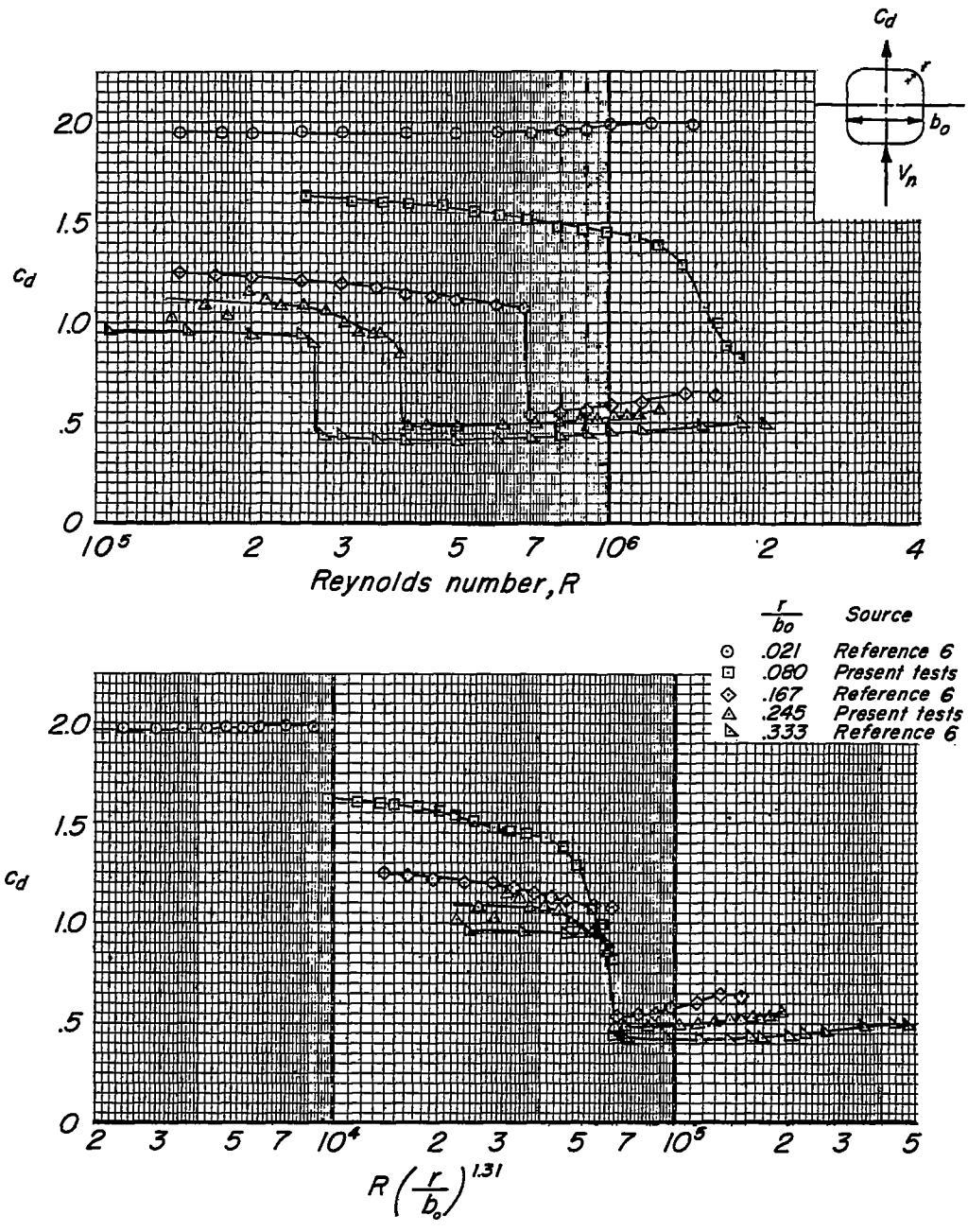

(a) Square.

Figure 9.- Effect of corner radius on the variation of the section drag coefficient of square and diamond cylinders with Reynolds number.

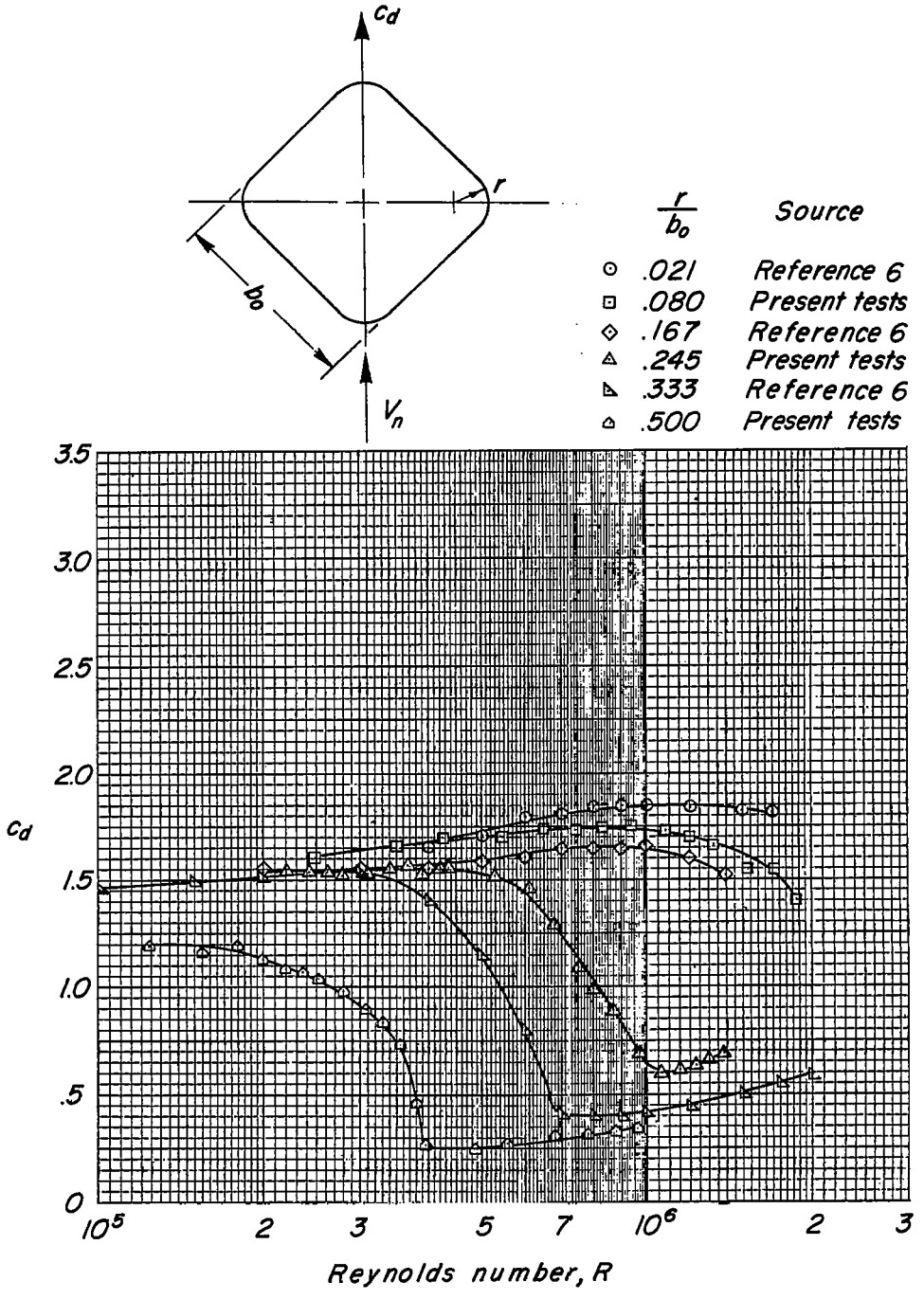

(b) Diamond. $\left(\text{Circle when } \frac{r}{b_o} = 0.500.\right)$

Figure 9.- Concluded.

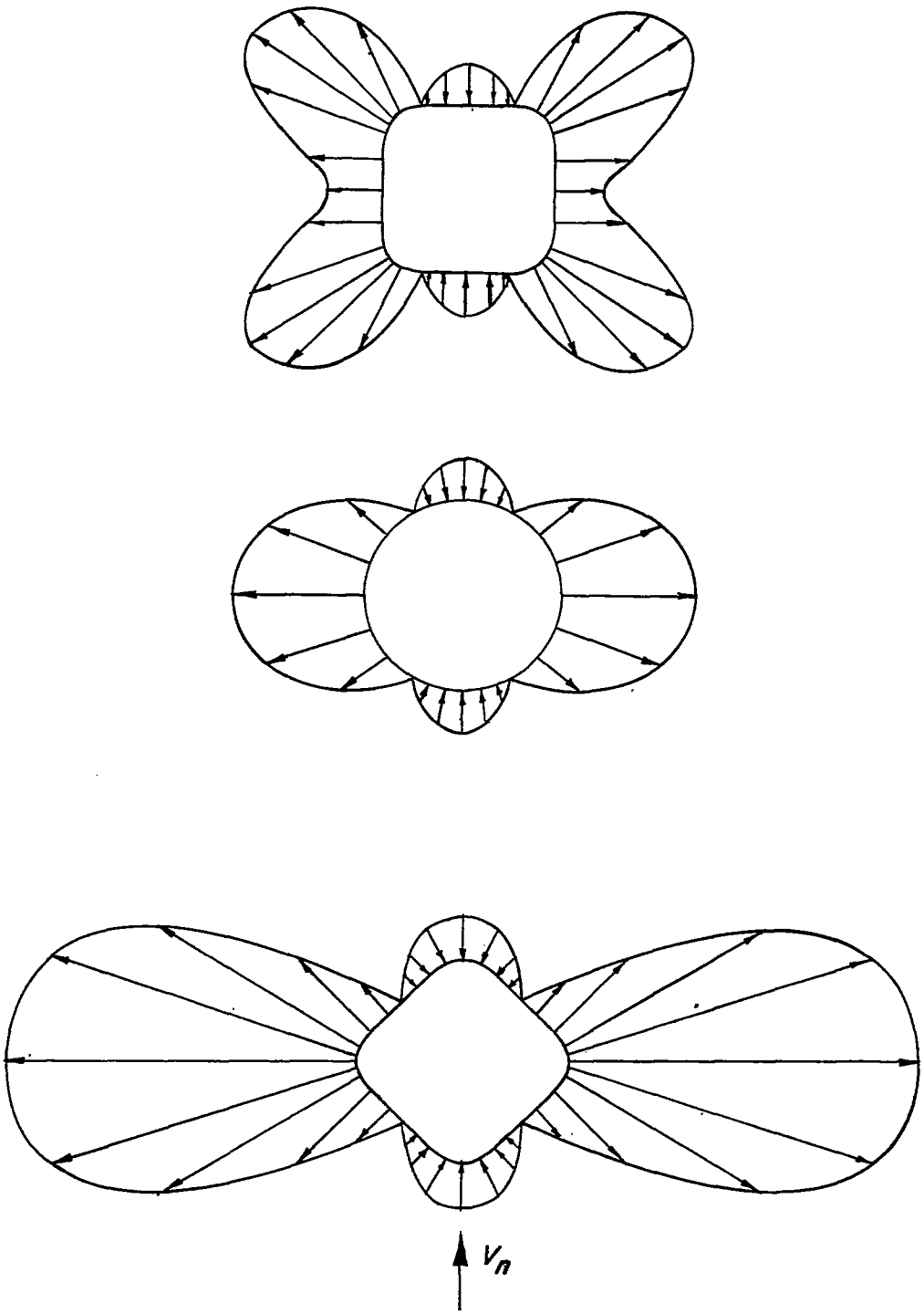

Figure 10.- Theoretical pressure distribution around various cross sections.

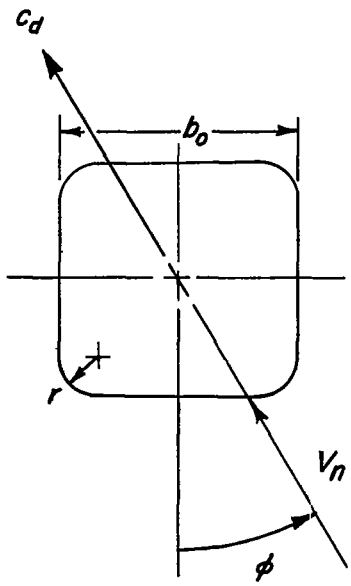

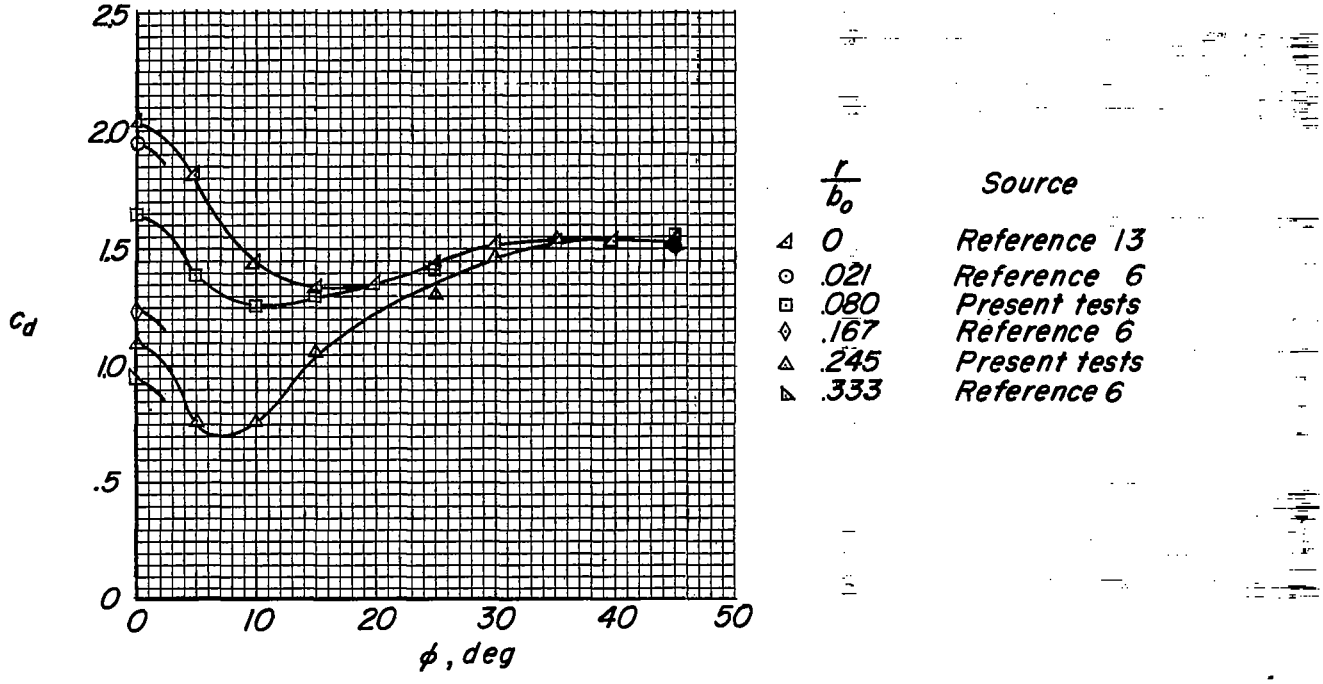

Figure 11.- Effect of incidence of flow and corner radius on the subcritical drag coefficient of square cylinders.

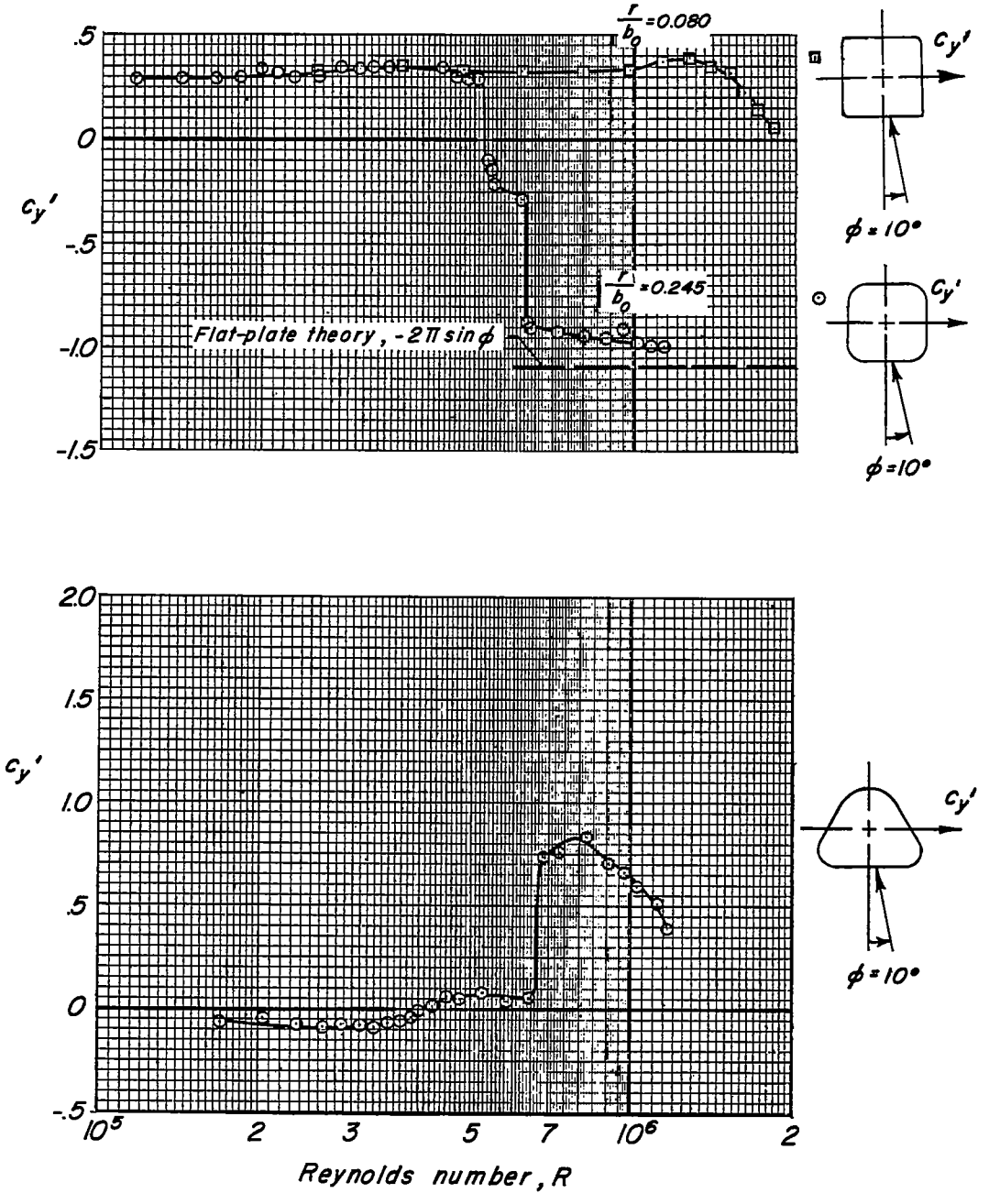

(a) Squares and triangle.

Figure 12.- Effect of cross section on the variation of section side-force coefficient with Reynolds number. ϕ = 10°.

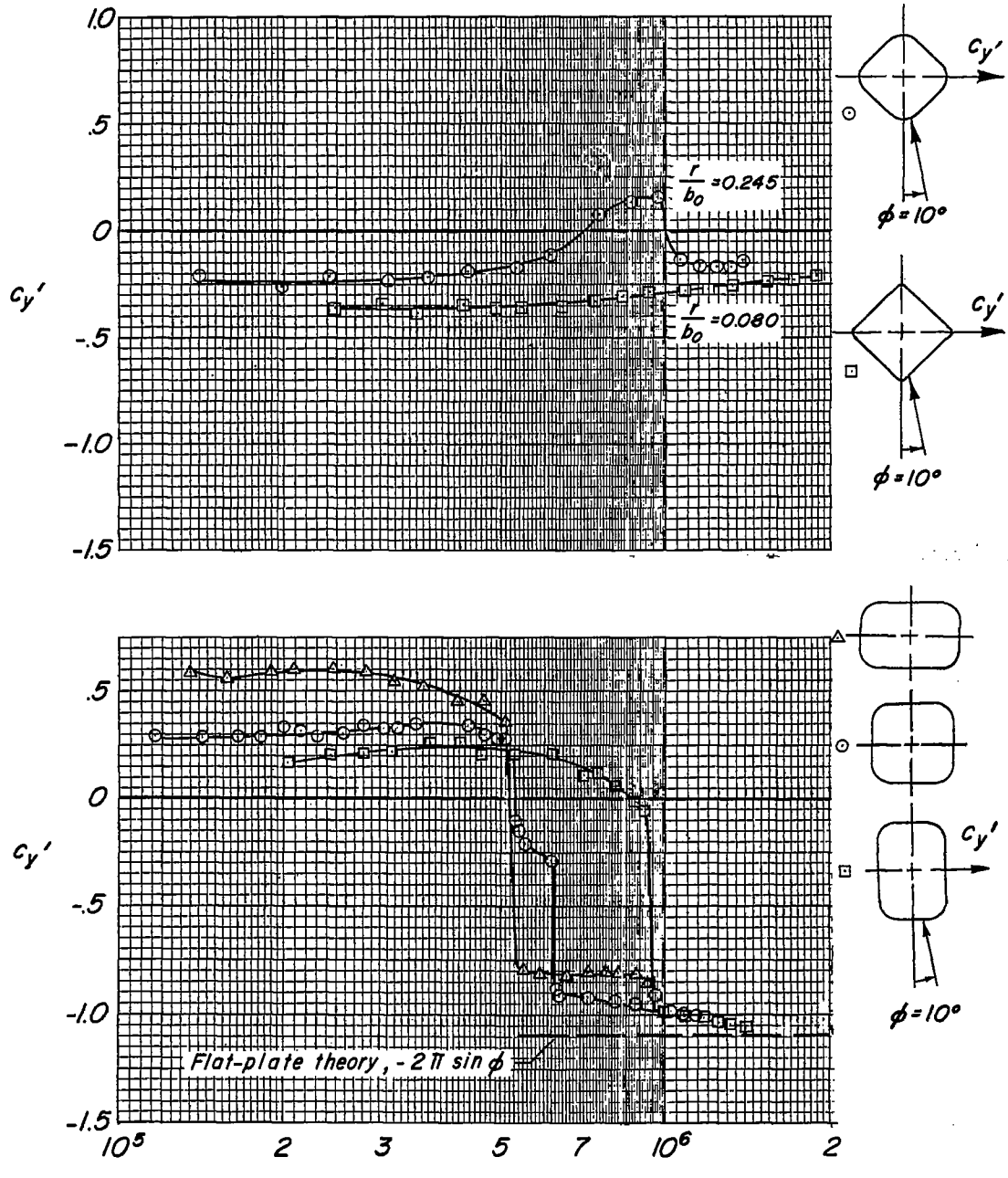

(b) Diamonds and rectangles.

Figure 12.- Continued.

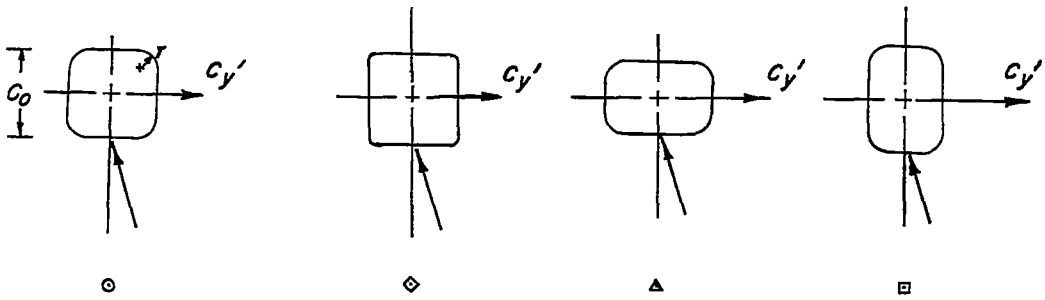

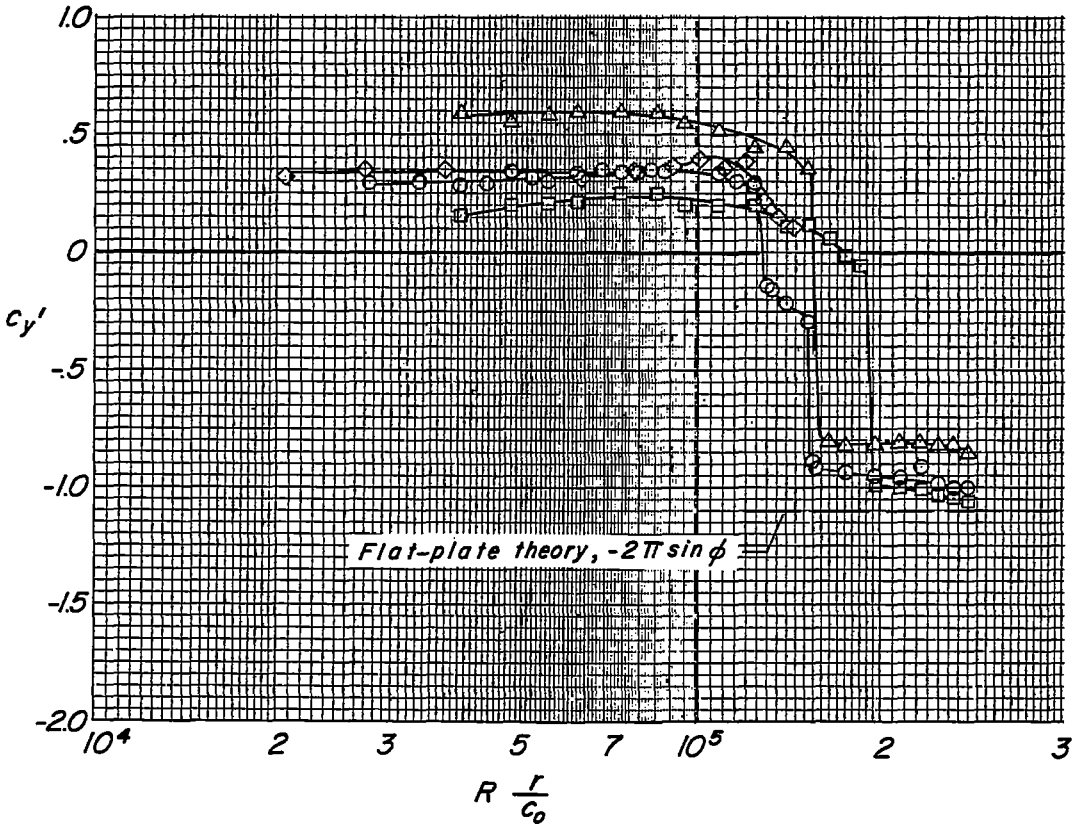

(c) Effect of Reynolds number based on corner radius.

Figure 12.- Concluded.

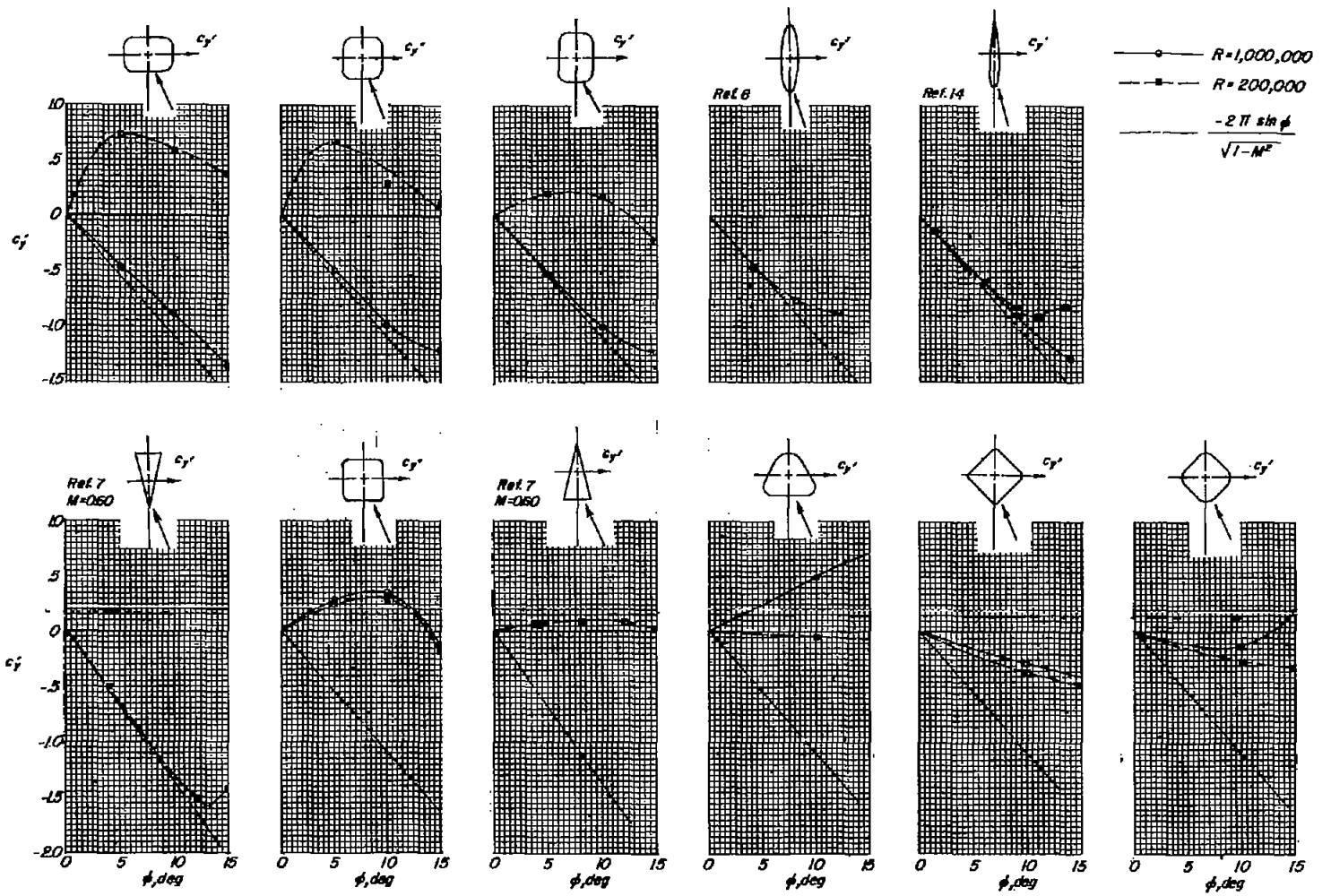

Figure 13.- Effect of cross section and flow incidence on the side-force coefficient. (Data are for incompressible flow unless otherwise noted.)

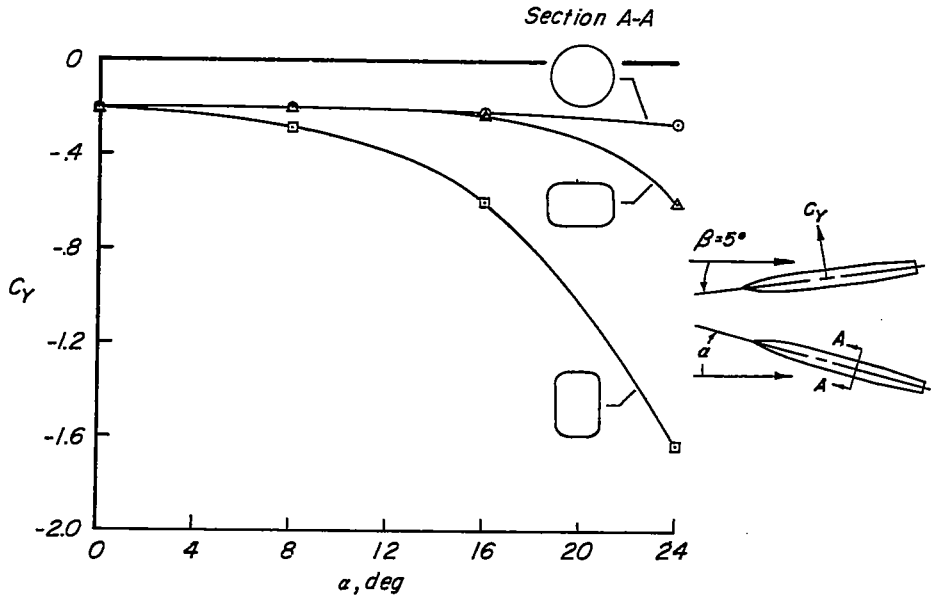

(a) Measured on three-dimensional bodies.

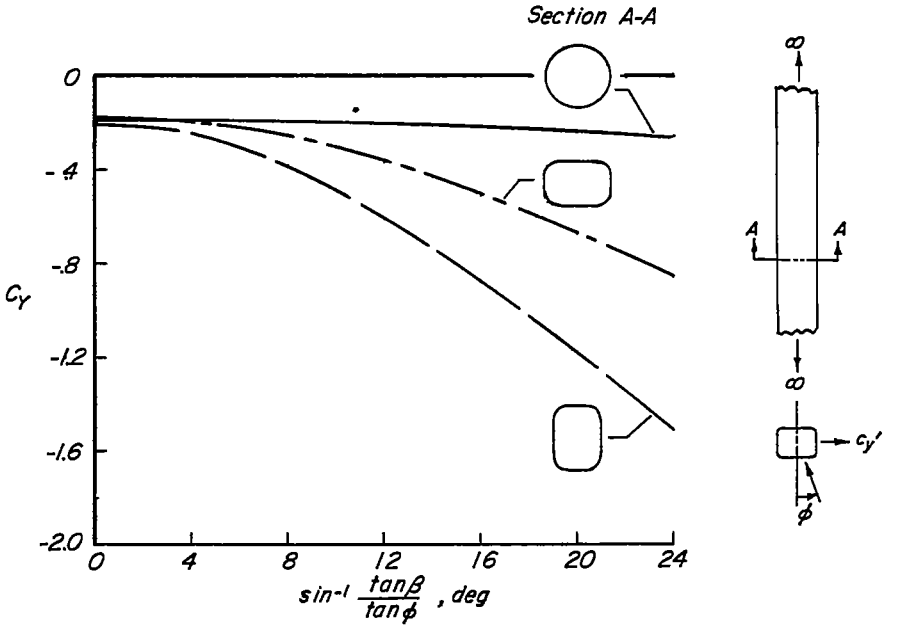

(b) Estimated from two-dimensional-cylinder data by using equations (3) and (4).

Figure 14.- Effect of fuselage cross section on side-force coefficient developed on three-dimensional body.

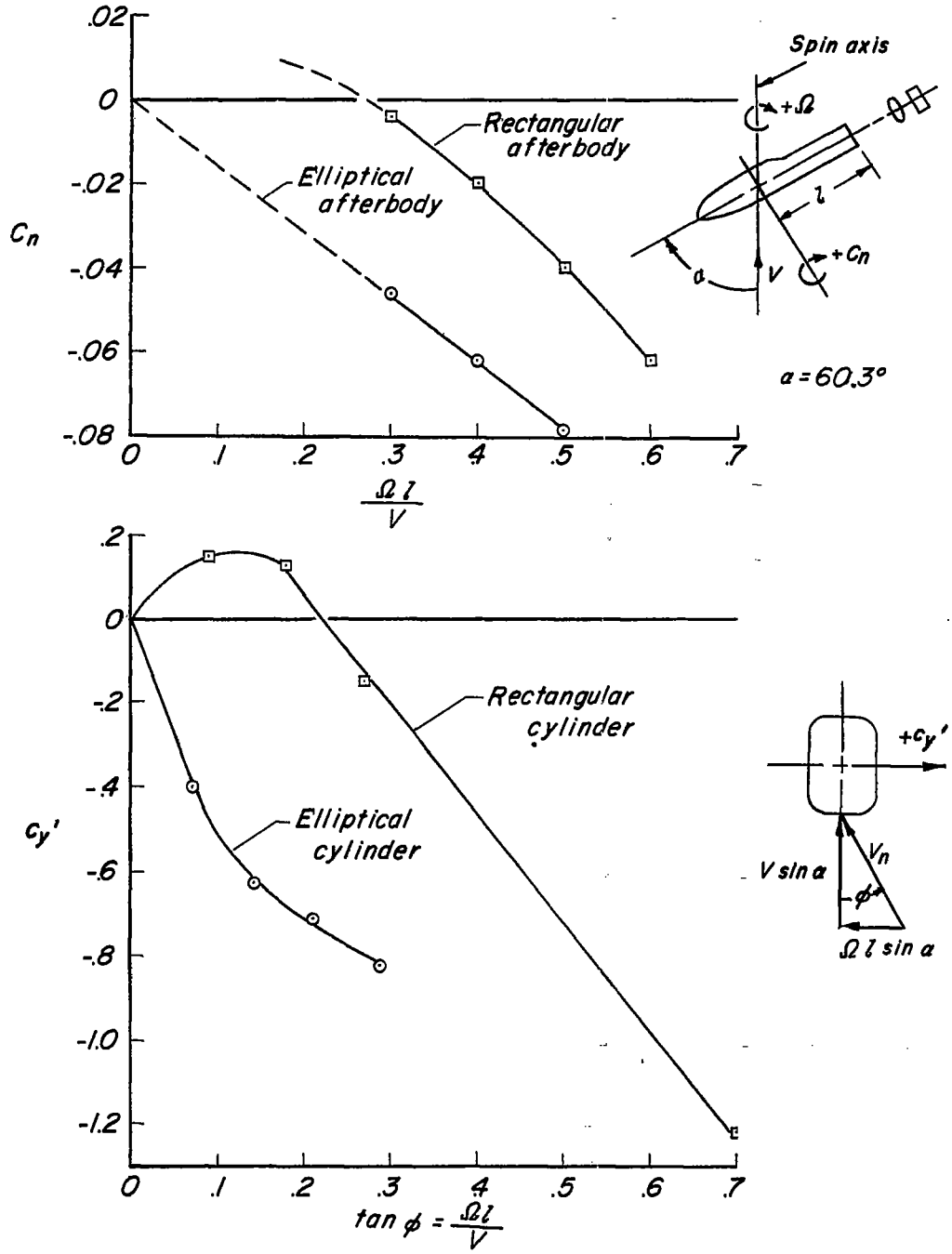

Figure 15.- Comparison of yawing-moment coefficient in spin (obtained from ref. 2) with side-force coefficient developed on two-dimensional cylinders.